International Journal of Bifurcation and Chaos, Vol. 14, No. 4 (2004) 1241–1266

CATASTROPHE THEORETIC CLASSIFICATION OF NONLINEAR OSCILLATORS

A. YU. KUZNETSOVA and A. P. KUZNETSOV
Institute of Radio-Engineering and Electronics of RAS, Saratov Division, Zelenaya 38, Saratov, 410019, Russia

C. KNUDSEN and E. MOSEKILDE
Department of Physics, The Technical University of Denmark, DK-2800, Kgs. Lyngby, Denmark

Received November 16, 2001; Revised March 12, 2003

Catastrophe theory is employed to classify different types of nonlinear oscillators, basing on the complication of their potentials. By using Thom's catastrophe unfoldings as oscillator potentials, we have introduced more general models to describe the dynamics of nonlinear oscillators, differing from each other by the form of their potential wells and by the possibility of escape. Spreading the investigation in the space of the parameters of the potential function, we have revealed that our examples defined via Thom's catastrophe unfoldings have some type of universal properties in the context of forced oscillations. For oscillators with nonescaping solutions, we have detected such typical bifurcation structures as crossroad areas and spring areas, and have described the universal scenario of their evolution under the forcing amplitude variation. On increasing the potential function degree, the complexity of the charts of the dynamical regimes results from the repetition of the described bifurcation scenario. For oscillators with escaping solutions, such general properties were investigated, as dependence of the charts of the dynamical regimes and the basins on the parameters of the potential function. We have observed that these properties are typical in a broad range of the control parameters.

Keywords: Space of parameters for the potential function; basin bifurcations; two-dimensional bifurcation diagrams; crossroad area–spring area transition.

1. Introduction

There are three basic motivations for studying the dynamics of nonlinear oscillators.

First, forced nonlinear oscillators, while remaining one of the simplest forms of nonlinear systems, yield a wide variety of interesting nonlinear phenomena such as regular and chaotic motions, coexisting attractors, regular and fractal basin boundaries and local and global bifurcations.

Second, the nonlinear oscillator example allows us to study the routes to complex dynamics from order to chaos. The type of equation for nonlinear oscillators considered in this work is given by

$$\ddot{x} + k\dot{x} + \frac{\partial U(x)}{\partial x} = B \cos \omega t \,, \qquad (1)$$

where $k > 0$ is the damping coefficient and $U(x)$ is the potential function. The right-hand side describes a harmonically varying periodic force. The case of $U(x) = x^2/2 + x^4/4$ was first investigated by Duffing [1918], who studied harmonic solutions. With the development of nonlinear dynamics, understanding of nonperiodic chaotic solutions has become possible [Ueda, 1992].

Table 1. Examples of oscillators with different kinds of potential function.

The kind of the potential function:		The examples:	
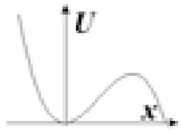	$U(x) = \frac{x^2}{2} - \frac{x^3}{3}$ $\ddot{x} + k\dot{x} + x - x^2 = B \cos \omega t$ (2)	Thompson, Soliman	Capsize model for a ship. Lateral vibrations of an axially compressed shell.
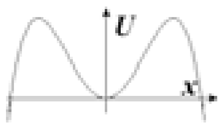	$U(x) = \frac{x^2}{2} - \frac{x^4}{4}$ $\ddot{x} + k\dot{x} + x - x^3 = B \cos \omega t$ (3)	Kao, Thompson and Stewart	The dynamics is similar to the forced pendulum near the potential minimum.
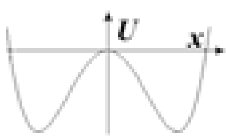 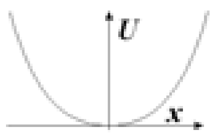	$U(x) = -\frac{x^2}{2} + \frac{x^4}{4}$ $\ddot{x} + k\dot{x} - x + x^3 = B \cos \omega t$ (4) $U(x) = \frac{x^2}{2} + \frac{x^4}{4}$ $\ddot{x} + k\dot{x} + x + x^3 = B \cos \omega t$ (5)	Guckenheimer and Holmes, Moon, Parlitz, English	Support column loaded beyond its buckling point. Magneto-elastic beam in the nonuniform field of two permanent magnets.
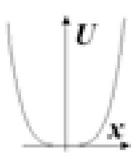	$U(x) = \frac{x^4}{4}$ $\ddot{x} + k\dot{x} + x^3 = B \cos \omega t$ (6)	Hayashi, Ueda, Mosekilde	Electrical circuit with magnetic saturation in core inductor.
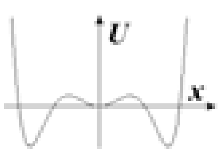	$U(x) = \frac{x_0^2 x^2}{2} - \frac{(x_0^2 + 1)x^4}{4} + \frac{x^6}{6}$ $\ddot{x} + k\dot{x} + x(x^2 - x_0^2)(x^2 - 1) = B \cos \omega t$ (7)	Li and Moon	Magneto-elastic beam in the nonuniform field of three permanent magnets.
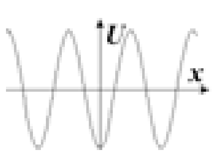	$U(x) = -\cos x$ $\ddot{x} + k\dot{x} + \sin x = B \cos \omega t$ (8)	MacDonald, Huberman, Swift	Periodically forced pendulum or Josephson junction.

Finally, as the third and perhaps most important motivation, nonlinear oscillators of the form (1) describe the dynamics of many real systems, for example, the dynamics of the forced pendulum [MacDonald & Plischke, 1983], a ball on a nonlinear spring and the unstable working regime of a synchronous motor [Goryachenko, 1995]. The nonlinear oscillator (1) can be used to model the capsize of a ship [Soliman & Thompson, 1991]. It also describes the dynamics of a support column loaded beyond its buckling point [Thompson & Stewart, 1986] and the magneto-elastic beam in the nonuniform field of two [Moon & Holmes, 1979] or three [Li & Moon, 1990] permanent magnets. It can describe the oscillations of a particle in a twin-well potential [Szemplinska-Stupnicka, 1993], the indeterminate jumps to resonance for nonlinear mechanical structures and electrical systems [Thompson *et al.*, 1987], a periodically forced suspended cable [Kloster & Knudsen, 1995], or the lateral vibrations of axially compressed shells [Thompson, 1995]. The nonlinear restoring force in Eq. (1) can represent the simplest form of magnetic saturation in an electrical circuit with a core inductor [Hayashi & Ueda, 1973]. Equation (1) can describe an electrical circuit with a ferroelectrical capacity [Petersson, 1990] as well as a variety of dissipative electrical circuits [Klinker *et al.*, 1984]. In a broader sense, it even models a variety of phenomena in physically extended systems, such as charge-density-waves in plasmas [Huberman & Crutchfield, 1979], four-wave interactions [Flytzanis & Tang, 1980], optical bistability [Goldstone & Garmire, 1984], and Josephson junctions [Huberman *et al.*, 1980].

Duffing's equation has been studied both theoretically and experimentally by many researchers. However, in spite of the considerable number of articles devoted to the study of nonlinear oscillators, there is not yet a single point of view of all phenomena. Hence, it is necessary to attempt a classification using a new unification approach.

In Table 1 we have summarized some examples of applications of Eq. (1) with different potentials. The table shows a sketch of the potential function, the corresponding dynamic equation, and the associated references. The hierarchy of models shown in the table are organized in accordance with an increasing degree of the polynomial potential functions, beginning with an oscillator with one potential well and one hill, and ending with an infinite order potential function.

Several possible classification principles have been suggested for nonlinear oscillators. First, Thompson and Stewart [1986], for example, considered the qualitatively different shapes of the anharmonic potentials. They differentiated the systems depending on whether the restoring force in Eq. (1) increases more or less rapidly than a linear function of the displacement (stiffening or softening spring, respectively). They discussed the cases corresponding to Eqs. (3)–(5) in Table 1 as well as the oscillator with periodic potential (8).

Second, Neimark and Landa [1987] surveyed a number of papers devoted to the investigation of Duffing's equation driven by a harmonic force with some constant component B_0

$$\ddot{x} + k\dot{x} + \alpha x + \beta x^3 = B_0 + B \cos \omega t \,, \qquad (9)$$

where α and β are parameters, that determine the form of the potential function. They emphasized works in which the different types of nonlinear function in Eq. (1) were considered: softening springs ($\alpha > 0$, $\beta < 0$), stiffening springs ($\alpha > 0$, $\beta > 0$), springs with zero linear stiffness ($\alpha = 0$, $\beta < 0$) and springs with negative linear stiffness ($\alpha < 0$, $\beta > 0$).

Third, Kao *et al.* [1988] considered Eq. (9) with $B_0 = 0$. They distinguished three types of the nonlinear function: with $\alpha \neq 0$, $\beta > 0$ corresponding to Eq. (5) or $\alpha = 0$, $\beta > 0$ corresponding to Eq. (6) in Table 1, with $\alpha < 0$, $\beta > 0$ corresponding to Eq. (4), and with $\alpha > 0$, $\beta < 0$ corresponding to Eq. (3). The solutions to the systems (4)–(6) are stable and nonescaping, because $U(x) \to \infty$ when $|x| \to \infty$. The amplitude of the solutions to Eq. (3), on the other hand, increases unlimitedly for some initial conditions, and $U(x) \to -\infty$ when $|x| \to \infty$. Thus, Kao *et al.* [1988] differentiated the oscillators depending on whether the system had escaping or nonescaping solutions.

All the classifications mentioned above regard the case of Duffing's equation, and do not regard the Eqs. (2) and (7), which are the important steps in the hierarchy of Table 1. In this work we would like to spread the investigation of the nonlinear oscillators in the space of parameters for the potential function and to establish a hierarchy of oscillators including all possible polynomial potentials and basing on the gradual complication of their dynamics. For this purpose a new approach to the classification of nonlinear oscillators is proposed, which takes its origin in Thom's catastrophe theory [Arnold *et al.*, 1999; Poston & Stewart, 1978]. According to this scheme there are thirteen classification forms for families of smooth functions $\mathbb{R}^n \to \mathbb{R}$ with less than six parameters (see Thom's classification theorem [Bröcker & Lander, 1975; Lu, 1976]). The first four elementary catastrophes of the scheme are summarized in Table 2.

Consideration of the nonlinear oscillator equation in the context of catastrophe theory was carried out by other authors. Using Duffing's

Table 2. Thom's elementary catastrophes.

Catastrophe	Codimension r	Function	
Fold	1	$U(x) = x^3 + ax$	(10)
Cusp	2	$U(x) = \pm(x^4 + ax^2 + bx)$	(11)
Swallowtail	3	$U(x) = x^5 + ax^3 + bx^2 + cx$	(12)
Butterfly	4	$U(x) = \pm(x^6 + ax^4 + bx^3 + cx^2 + dx)$	(13)

equation to model the passing of seismic waves in the asthenosphere, Mitra and Sinha [1981] observed the existence of two cusp catastrophes in parameter space. Moreover, Saunders [1980], considering Duffing's equation as a couple of cusp catastrophes, supposed that if one adds further odd powers of x to the restoring force of the Duffing equation, then one can obtain higher order catastrophes. This way we are going to carry out our research. Introducing the different forms of the nonlinear restoring force in Eq. (1), we shall observe different catastrophes and their influence on system dynamics. In this work the catastrophe means a sudden transition from one state of minimum potential, one stable equilibrium, to another [Woodcock & Davis, 1991].

Using the catastrophe unfoldings as oscillator potentials, we obtain a more general classification scheme, because each of the potential functions in Table 1 may be transformed into a canonical type of some elementary catastrophe in Table 2. The introduced classification arranges the oscillators from simple to more complicated potential according to the number of the parameters. This allows us to investigate the dynamics of the oscillators in the whole parameter space. The codimension of the catastrophe (here the number of controlling parameters in the potential function shown in Table 2) increases from stage to stage in our study. We shall begin with the oscillator with one parameter, which corresponds to the fold catastrophe, and finish with the four-parameter oscillator corresponding to the butterfly catastrophe.

The advantages of this new classification are the following. First, different nonlinear oscillators studied earlier by many researches at fixed parameters of the nonlinearity show up as particular cases of the oscillators with catastrophe unfoldings. For example, the Thompson's model (2) is an oscillator with fold catastrophe at the parameter of the nonlinearity $a = 0.25$; the oscillator models (3)–(6) presented in works by Parlitz, Ueda, and others represent cases of the oscillator with cusp catastrophe at fixed potential function parameters; the model in Moon's study (7) is the simplest case of the oscillator with butterfly catastrophe. Thus, our examples, introduced via the catastrophe unfoldings, can be regarded as more general models. The above classification allows us to predict the kind of dynamics that we can expect for the oscillator with any polynomial potential function by considering the relevant class of oscillator with catastrophe.

Second, we have revealed that our examples defined via Thom's catastrophe unfoldings have some type of universal properties in the context of forced oscillations. We have divided different catastrophe unfoldings of oscillator potentials in two groups according to the general properties of oscillator dynamics: the oscillators with escaping solutions described in Sec. 2, and the oscillators with nonescaping solutions described in Sec. 3. For the first group, such general properties were investigated, as dependence of the charts of the dynamical regimes and the basins on the parameters of the potential function. For the second group of the oscillators, we have detected such typical bifurcation structures as crossroad areas and spring areas in the space of the parameters of the potential function, and we have described a universal scenario for their evolution under the forcing amplitude variation (see Sec. 3.1). This scenario is the same in different cases of the catastrophe unfoldings, and it repeats itself with increasing forcing amplitude. Guided by the catastrophe theory scheme, we have investigated the influence on the system dynamics of an increase in the degree of the potential function. The higher the degree of the polynomial potential function, the higher the speed of the development of this scenario, and the more times the scenario repeats itself. For the oscillators with higher degree potentials, the complexity of the charts of the dynamical regimes results from the repetition of the described bifurcation scenario.

Finally, using the catastrophe theory as a classification principle for the oscillators helps us to predict the areas in the space of the potential function parameters, which are interesting to study. We have observed in our investigations of oscillators with all of Thom's elementary catastrophes that if the parameters of the system are chosen far from the bifurcation manifold of the catastrophe, then the solution of the system is the simplest — a limit cycle, corresponding to the forced oscillations, but if the parameters are taken on or near the bifurcation manifold of the catastrophe, the solution can be a strange attractor, and the system has a rich bifurcation behavior. Thus, the complex dynamics is realized in the parameter spaces only near the bifurcation manifolds of the catastrophes. It is our main criteria for choosing ranges of the parameters of the potential function. The catastrophe theory can also help us estimate the location of a strange attractor in the phase space. For the system with potential of degree p in the form of the Thom's catastrophe Marzec and Spiegel [1980] observed that location of the strange attractor in the particular phase space involves the catastrophe set of a "potential" of degree $p+1$.

Before we begin our study, we need to explain the choice of the values of the forcing frequency and amplitude. In our work we have observed that the described universal properties are typical for a broad range of the control parameters. The typicalness of the presented bifurcation sets in the parameter space is due to the features of the considered oscillators. Choosing any forcing frequency, we can observe the general picture of the system dynamics. This results from the influence of the nonlinear shift of the natural frequency of the oscillator. The concept of natural frequency in our examples is not trivial, because there are no oscillations in the absence of the external forcing. Resonance properties appear in these systems in the presence of a harmonic external forcing. When there are terms in the oscillator equation with coordinate in higher than first degree, then these terms can be interpreted as nonlinear shift of the natural frequency. Thus, the natural frequency will depend on the amplitude of oscillations as determined by the amplitude of the external forcing. The mutual dependence of amplitude and frequency properties of the system allows us to pass through all characteristic regimes by varying the forcing amplitude at a constant forcing frequency. The inclination of synchronization areas on the plane of forcing frequency versus amplitude, as shown, for example, for Duffing's oscillator [Parlitz, 1991], serves as an illustration of this effect. Except for insignificant areas at small forcing frequencies, which correspond to atypical system regimes, we can pass through all the characteristic regimes with any choice of the forcing frequency. Our numerical investigations also testify that the variations of the charts of the dynamical regimes are insignificant in other ranges of the forcing frequency.

2. Dynamics of Nonlinear Oscillators with Escape

Let us first consider nonlinear oscillators with escaping solutions, potential functions of which obey the general rule $U(x) \to -\infty$, when $|x| \to \infty$. Examples of such oscillators are Eqs. (2) and (3) in Table 1. The equations considered in our study correspond to the fold catastrophe (10), the dual cusp catastrophe (11), and the swallowtail catastrophe (12).

2.1. *Dynamics of nonlinear oscillator with fold catastrophe*

The equation for the forced oscillator with fold catastrophe is

$$\ddot{x} + k\dot{x} - x^2 + a = B\cos\omega t\,. \tag{14}$$

The fold catastrophe is characterized by the merging and disappearance of the stable and unstable states of the system when the parameter a is changed. Notice, that the replacement $x \to x + 1/2$ in Eq. (2) in Table 1 leads to Eq. (14) with the parameter $a = 0.25$. Consequently, the well-known results from the works of Thompson [1995] and Soliman [1994], concerning the stability of ships in the sea, correspond to a single point on the a-axis. The solutions to this system possess the possibility of escape from the potential well for some initial conditions, or they can be attracted to a large amplitude orbit, due to a jump to resonance. In Fig. 1 we have shown the different basins of attraction, where the white color denotes the region of the escaping solutions and the black color corresponds to the region of the stable solutions with finite amplitude. A small increase in the forcing amplitude leads to a fractalization of the basin boundary [Thompson *et al.*, 1987], in which "white fractal fingers" of the escaping basin incurs into the black region [see Figs. 1(a) and 1(b)] . This is due to the homoclinic

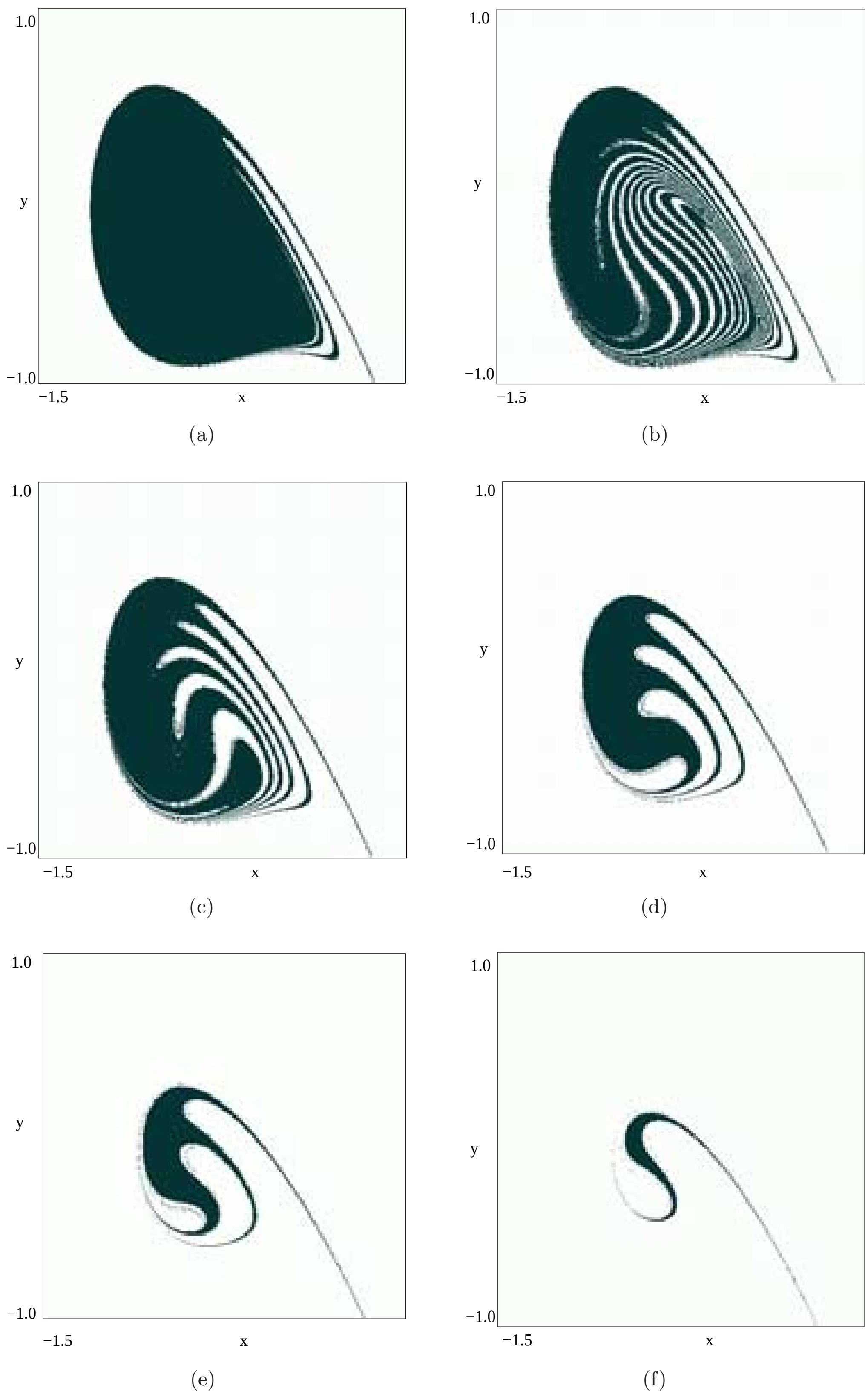

Fig. 1. Basin erosion sequence for the oscillator with fold catastrophe (14) showing the incursion of "fractal fingers" into the safe basin of nonescaping initial conditions (black) at $k = 0.1$, $\omega = 0.85$ and following parameter values: (a) $a = 0.25$, $B = 0.0725$, (b) $a = 0.25$, $B = 0.0750$, (c) $a = 0.2$, $B = 0.0725$, (d) $a = 0.15$, $B = 0.0725$, (e) $a = 0.1$, $B = 0.0725$, and (f) $a = 0.05$, $B = 0.0725$.

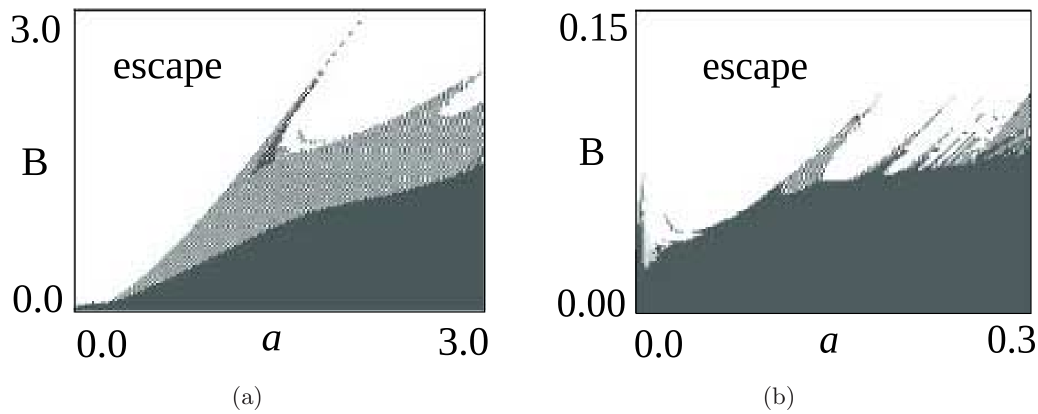

Fig. 2. Charts of the dynamical regimes for the oscillator with fold catastrophe (14) at initial conditions $x(0) = y(0) = 0.0$, $k = 0.1$ on the (amplitude, parameter a) plane in the cases (a) $\omega = 1.0$ and (b) $\omega = 0.85$.

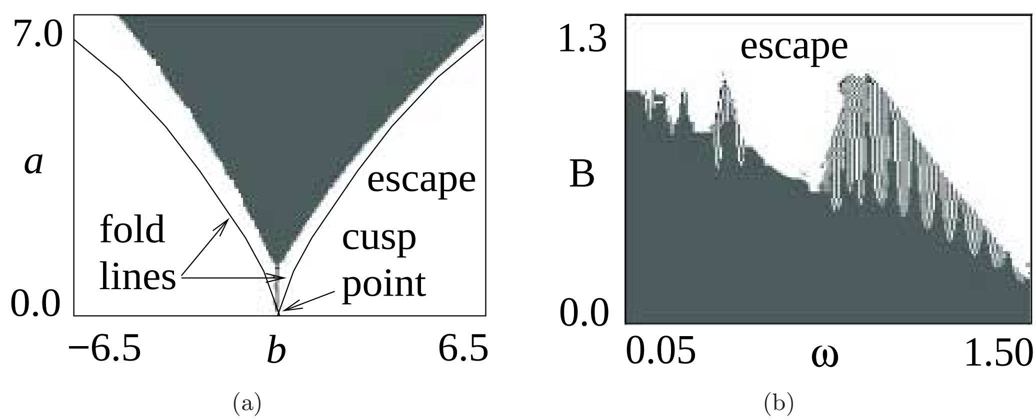

Fig. 3. Charts of the dynamical regimes for the oscillator with the dual cusp catastrophe (15) (a) on the (a, b)-plane at $k = 0.1$, $\omega = 0.85$ and $B = 0.1$, (b) on the (amplitude, frequency) plane at $k = 0.1$, $a = 4.03$, $b = 2.14$.

tangles of the stable and unstable manifolds of the hilltop saddle cycle at the chaotic saddle bifurcation [Thompson, 1995]. If we fix the forcing amplitude B and slowly decrease the parameter a, the same sequence of basin erosions occurs, which ultimately leads to the disappearance of the basin of attraction for the stable nonescaping solution [see Figs. 1(c)–1(f)].

To illustrate how this happens, charts of the dynamical regimes were plotted on the plane of the forcing amplitude and the parameter a [see Figs. 2(a) and 2(b)]. The escape region is shown as white, gray color corresponds to the stable period-1 solutions, and light gray marks the boundary between the regions of escaping and nonescaping solutions, which seems to be fractal. Figure 2(b) shows an enlarged fragment of the fractal boundary. The smaller the value of the parameter a, the smaller the value of the forcing amplitude will be for the boundary. If one plots also the charts of the dynamical regimes on the plane of the forcing amplitude versus frequency at different values of the parameter a, one can observe that the reduction of this parameter lead to the displacement of the escape boundary in the region of low amplitude and low frequency [Kuznetsov & Potapova, 2000].

Analogous charts of the dynamical regimes were obtained for other values of the forcing frequency.

2.2. *Dynamics of nonlinear oscillator with dual cusp catastrophe*

The equation of the oscillator with a dual cusp catastrophe [Woodcock & Davis, 1991] is

$$\ddot{x} + k\dot{x} - x^3 + ax + b = B \cos \omega t\,. \tag{15}$$

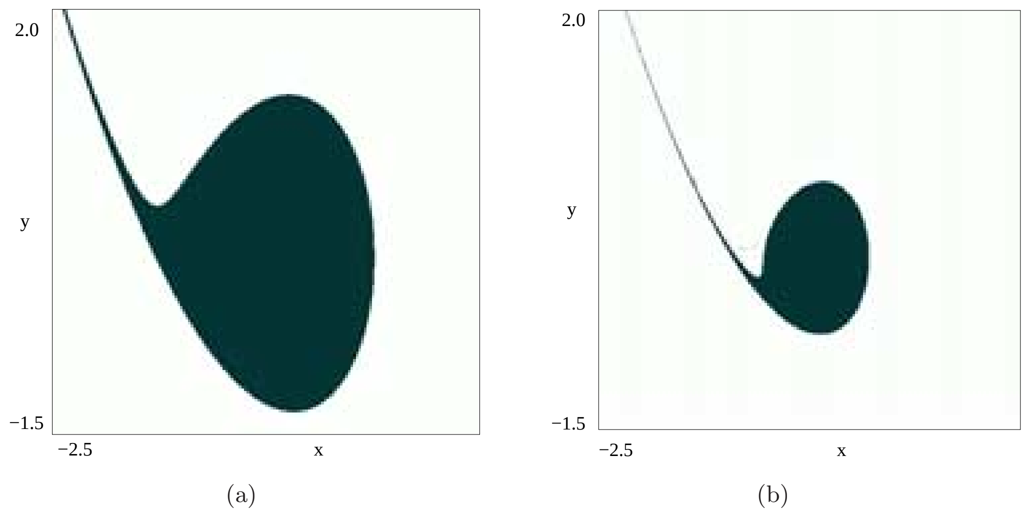

Fig. 4. Contraction and disappearance of the basin of the nonescaping solution for the oscillator (15) at $k = 0.1$, $B = 0.1$, $\omega = 0.85$, $b = 2.14$ at the decreasing of parameter a: (a) $a = 4.03$ and (b) $a = 3.50$.

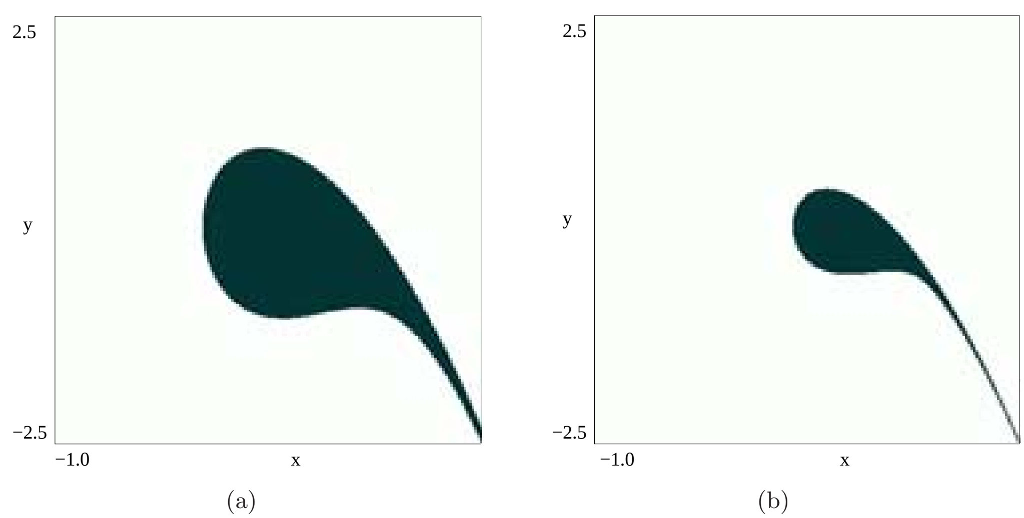

Fig. 5. Contraction and disappearance of the basin of nonescaping solution for the oscillator (15) at $k = 0.1$, $b = 0.0$, $\omega = 0.85$, $a = 4.3$ with increasing forcing amplitudes B: (a) $B = 2.5$ and (b) $B = 2.9$.

Its potential (11) differs from the potential in Eq. (3) of Table 1 due to the introduction of the parameters a and b, variation of which changes the deepness and the symmetry of the well. With the forcing amplitude $B = 0$ there is a cusp point in the (a, b)-plane, where two-fold lines emanate [see Fig. 3(a)]. On these lines the potential has an inflection point. These curves bound the region of potential functions with two hills and one well and pass close to the boundary of the triangular region of nonescaping period-1 solutions shown as gray in Fig. 3(a).

As for the preceding case, the charts of the dynamical regimes for this oscillator in the (B, ω) plane show a fractal boundary between the escape region and stable solution region [see Fig. 3(b)]. This boundary moves towards the region of smaller forcing amplitudes and frequencies, contracting the area of nonescaping solutions in size, as the parameter a is decreased or the parameter b is increased. When decreasing parameter a from 4.03 to 3.50, the basin transformations shown in Fig. 4 take place. Increasing of parameter b, from 2.14 to 2.8, for example, leads to the same contraction and subsequent disappearance of the region of the nonescaping solutions. The basin transformations as a function of forcing amplitude are shown in Fig. 5, where the basin is observed to decrease signifi-

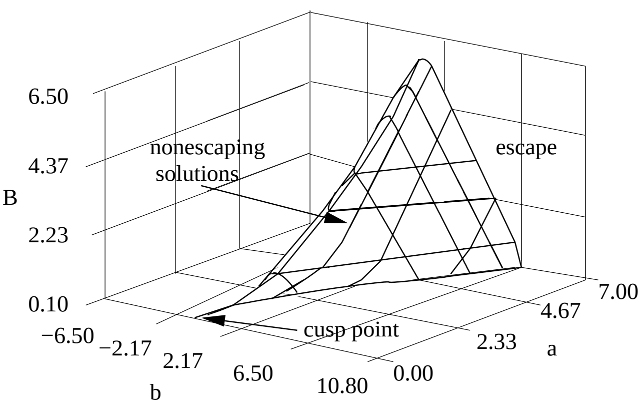

Fig. 6. Division of the parameter (a, b, B) space for the oscillator (15) into the regions of characteristic dynamics for $k = 0.1$ and $\omega = 0.85$.

cantly with increasing forcing amplitudes to disappear completely for $B \approx 3.0$.

The regions of the stable and unstable regimes in the three-dimensional parameter space (B, a, b) are shown in Fig. 6. This three-dimensional chart was reconstructed from a number of two-dimensional sections, as indicated in the figure. All sections exhibit a triangle shape. For example, the basis of this figure is the triangular region of nonescaping solutions shown in Fig. 3(a). The area of nonescaping solutions arise from the cusp point at $a = b = B = 0$ and become larger with increasing parameters. All points inside this figure correspond to stable period-1 solutions. For simplicity, all escape boundaries are shown schematically to be smooth in Fig. 6. When considered in more detail, they have a fractal structure, which is more noticeable at small values of the parameter b.

The two-dimensional sections exhibit the same triangle shape at other values of the forcing frequency, so we expect the same form of the three-dimensional chart.

2.3. *Dynamics of nonlinear oscillator with swallowtail catastrophe*

The following by its complicity potential (12) in our scheme can have two hills and two wells, one hill and one well, or no critical points. For the whole picture of all possible forms of the potential, which correspond to the different points of the bifurcation set of the swallowtail we refer to [Bröcker & Lander, 1975]. For the oscillator with the swallowtail catastrophe the dynamic equation reads

$$\ddot{x} + k\dot{x} + x^4 + ax^2 + bx + c = B \cos \omega t \,. \quad (16)$$

We investigate the dynamics in the space of the parameters of the potential chosen near the bifurcation set. The corresponding regions of stable and unstable regimes in the three-dimensional parameter space (a, b, c) are shown in Fig. 7. This three-dimensional chart was reconstructed from a number of two-dimensional slices. At the top of the figure there is a large region of escaping solutions, with right-hand edges corresponding to the bifurcation set of the swallowtail [Bröcker & Lander, 1975]. This form of the surface follows from the potential's transformations. At large values of the parameter b, the oscillator potential has at least one well for any a and c, so there are no escaping solutions in the system. On the other hand, at large negative b there is no stable equilibrium possible above the surface, and one stable equilibrium below the escape boundary at $c \approx 2$ (see Fig. 7). The corresponding basin erosion sequence is depicted in Fig. 8, where the fractalization of the basin boundary due to the heteroclinic intersections of saddle manifolds can be seen for increasing values of c. The same basin erosion sequence happens, for example, when parameter b is reduced from 0.05 to 0.005.

Analogous dynamics is observed for other values of the forcing frequency.

Thus, we have illustrated for oscillators with escaping solutions, i.e. with potentials corresponding to the fold, the dual cusp and the swallowtail catastrophes, such general properties, as the dependence of the escape boundary of the charts of the dynamical regimes on the potential function parameters and the basin erosion sequence under variation of the nonlinear parameters. We have observed the same results at other values of the forcing frequency. We expect similar dynamical properties for the oscillators with higher order catastrophes which have escaping solutions.

3. Dynamics of Nonlinear Oscillators with Nonescaping Solutions

3.1. *Dynamics of nonlinear oscillator with cusp catastrophe*

Let us consider the behavior of a nonlinear oscillator with cusp catastrophe whose dynamics is governed

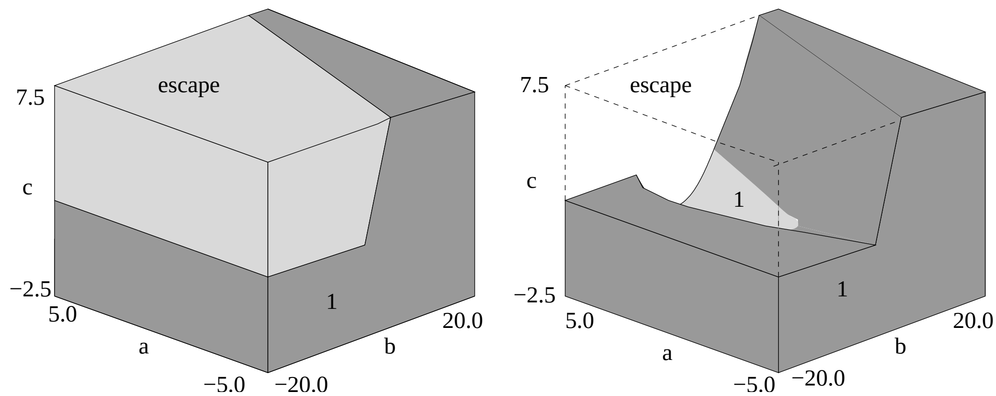

Fig. 7. Division of the parameter (a, b, c) space on the regions of characteristics dynamics for $B = 0.1$, $k = 0.1$ and $\omega = 0.85$ for the oscillator with the swallowtail catastrophe (16). In the left figure the escape region is cut out from the cub in order to show its inner structure.

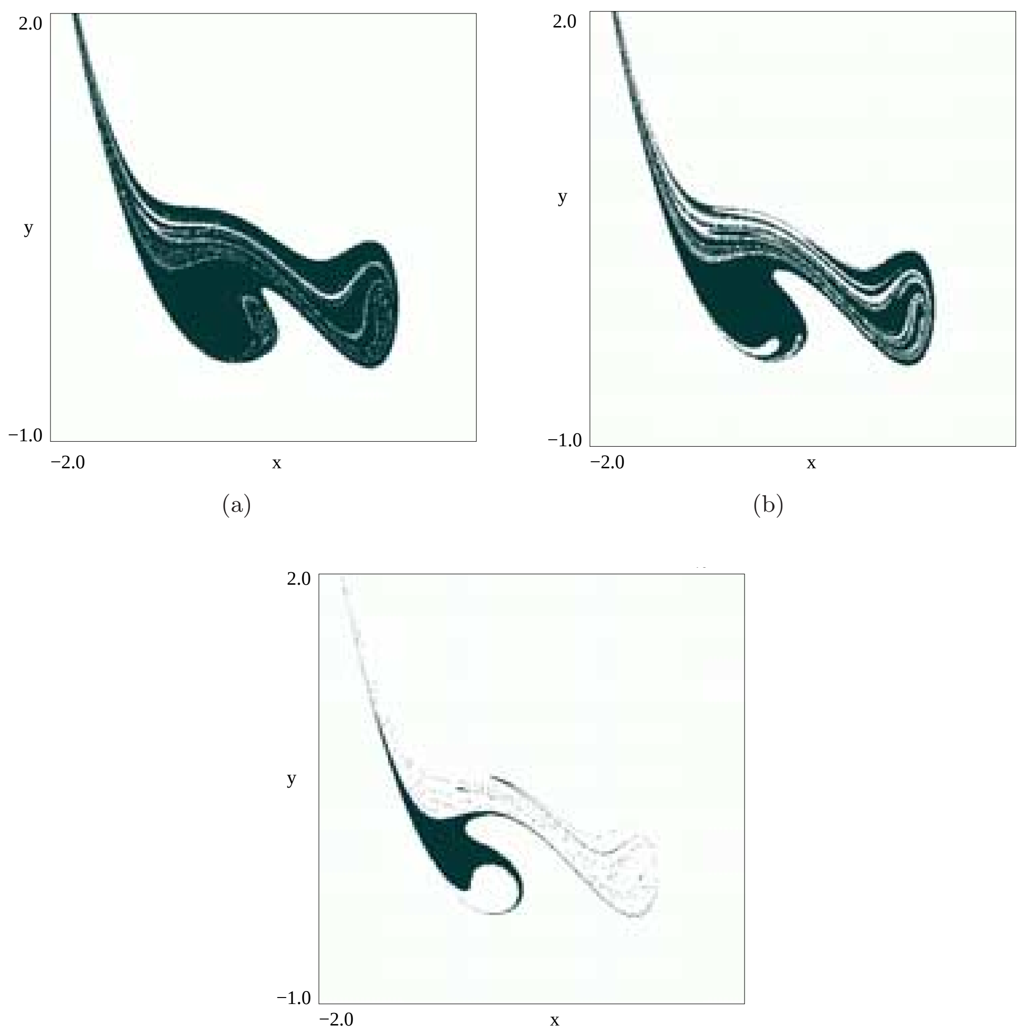

Fig. 8. Basin erosion sequence at $k = 0.1$, $B = 0.1$, $a = -1.0$, $b = 0.0$ and $\omega = 0.85$ under the increasing of c: (a) $c = 0.105$, (b) $c = 0.120$, and (c) $c = 0.140$.

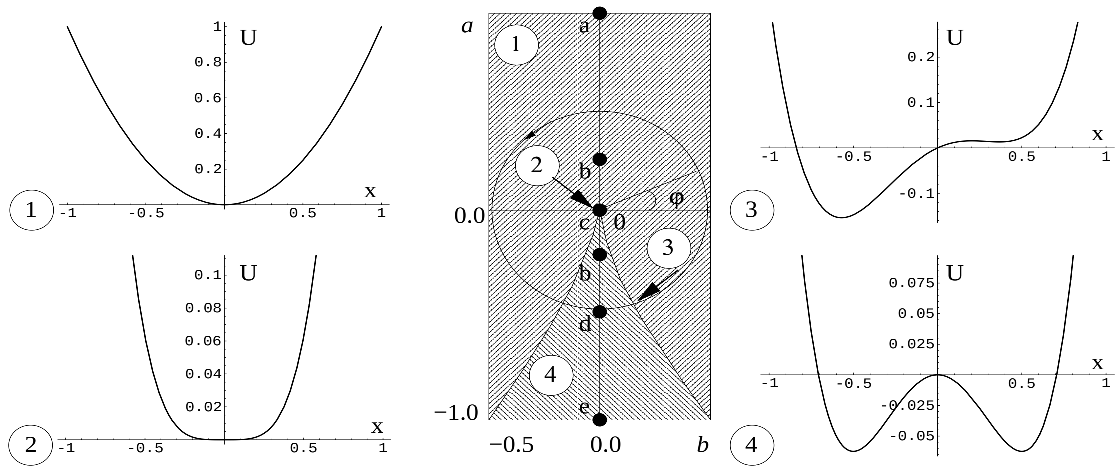

Fig. 9. Fold lines and cusp point for the oscillator with the cusp catastrophe (17) on the (b, a)-plane. Outlined points of the parameter plane correspond to the previous studies of the oscillator (17): a in [Parlitz, 1991], b in [Thompson & Stewart, 1986], c in [Ueda, 1991], d in [Szemplinska-Stupnicka, 1993], and e in [English & Lauterborn, 1991].

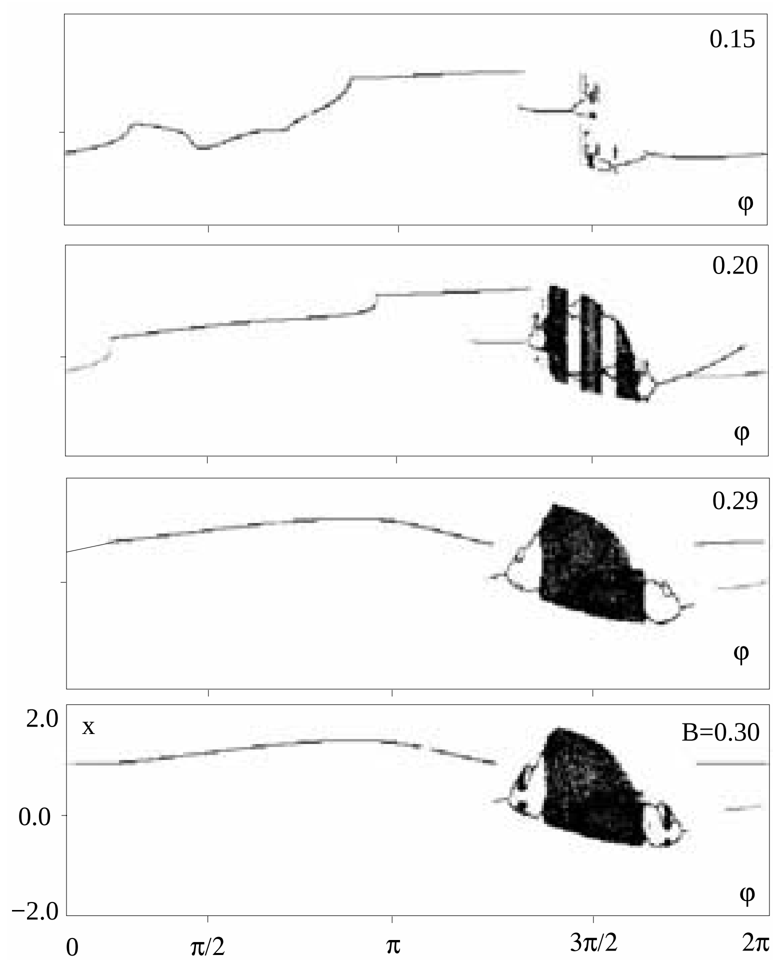

Fig. 10. The sequence of the bifurcation diagrams for Eq. (17) at $k = 0.2$, $\omega = 1.0$, $x_0 = 3.1$, $y_0 = 3.1$, and increasing amplitude B from 0.15 to 0.3. Each diagram corresponds to a scan of the circle $R = 0.5$ on the (b, a)-plane.

by

$$\ddot{x} + k\dot{x} + x^3 + ax + b = B \cos \omega t\,. \tag{17}$$

This system has a cusp point [Poston & Stewart, 1978] at the origin ($a = b = 0$) in the two-parameter plane from which two-fold lines emanate (see Fig. 9).

These lines form the boundaries of the region of the two-well potential (11). The dynamics of this system was studied by different authors [Thompson & Stewart, 1986; Szemplinska-Stupnicka, 1993; Parlitz, 1991; English & Lauterborn, 1991; Ueda, 1991] at several sample points of the parameter plane (outlined in Fig. 9). Let us now consider the dynamical regimes in the vicinity of the cusp point. In Fig. 10 we have presented a sequence of one-dimensional bifurcation diagrams for Eq. (17). Each diagram corresponds to a closed path around the cusp point in the (b, a)-parameter plane parameterized by an angle φ, (see Fig. 9). The forcing amplitude B was fixed with different values in the different panels. A saddle-node bifurcation occurs at small values of $B = 0.05$ and for $\varphi \approx 3\pi/2$. This angle corresponds to a domain of coexisting orbits in the parameter plane. Increasing the forcing amplitude leads to the appearance of several saddle-node bifurcations. The first period-doubling bifurcation occurs just before the parameter value $B = 0.15$. For forcing amplitudes $B > 0.16$ the attractor can become chaotic via a period-doubling cascade (see figure). Periodic windows can be observed in the region where chaotic solutions are found (large values of φ). A further increase in B leads to the disappearance of the period-3 and period-4 windows (most visible at $B = 0.20$). At $B = 0.29$ a so-called period-bubbling is seen, i.e. both period-doubling and period-halving [English & Lauterborn, 1991]. A final increment of the forcing amplitude to $B = 0.30$ reveals that there are now complete period-doubling cascades to chaos in the place of each bubble.

In the parameter plane, several typical configurations of the flip and fold bifurcation lines can be distinguished in the stability domains of periodic regimes (Fig. 11). They are organized around a codimension-two cusp bifurcation point. The first configuration is a so-called "crossroad area" [Mira & Carcasses, 1991]. The second configuration, which has been termed a "spring area" [Mira & Carcasses, 1991], involves codimension-two flip bifurcation points where tangent points of flip and fold bifurcation lines meet. For transitions between these configurations we refer to the paper by Carcasses and Mira [1991]. In Fig. 11 two crossroad areas and one spring area are shown. The largest crossroad area involves the subharmonic of type (n, m). (The subharmonic n/m means that the system accomplishes n oscillations during m periods of the external forcing [Ueda, 1991].) Another crossroad area, located in the right-hand part of figure, involves the $(2n + 1, 2m)$ subharmonic. Finally, the spring area is based on the $(2n - 1, 2m)$ subharmonic, in the left-hand part. A location of smaller areas inside of a bigger crossroad area was described in the works by Parlitz [1991], and by Scheffczyk *et al.* [1991]. These configurations were shown typically to be met in the two-parameter analysis of nonlinear dynamic systems with discrete and continuous time [Parlitz, 1991; Scheffczyk *et al.*, 1991; Mackey & Tresser, 1987; Komuro *et al.*, 1991; Gallas & Catarina, 1993]. Scheffczyk *et al.* [1991], for example, described the appearance of these structures in different nonlinear dissipative oscillators: Toda system, Morse system, soft symmetric oscillator and Duffing oscillator.

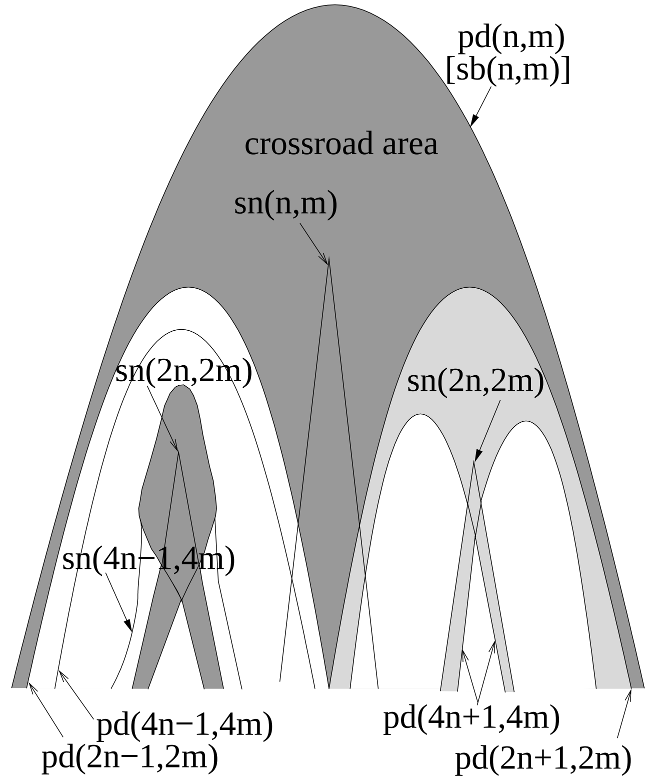

Fig. 11. The typical configurations of the flip and fold bifurcation lines "crossroad area" and "spring area" on the potential parameter plane. The "sn", "pd", and "sb" abbreviations correspond to the lines of saddle-node, period-doubling and symmetry breaking bifurcations and (n, m) define the involved subharmonics.

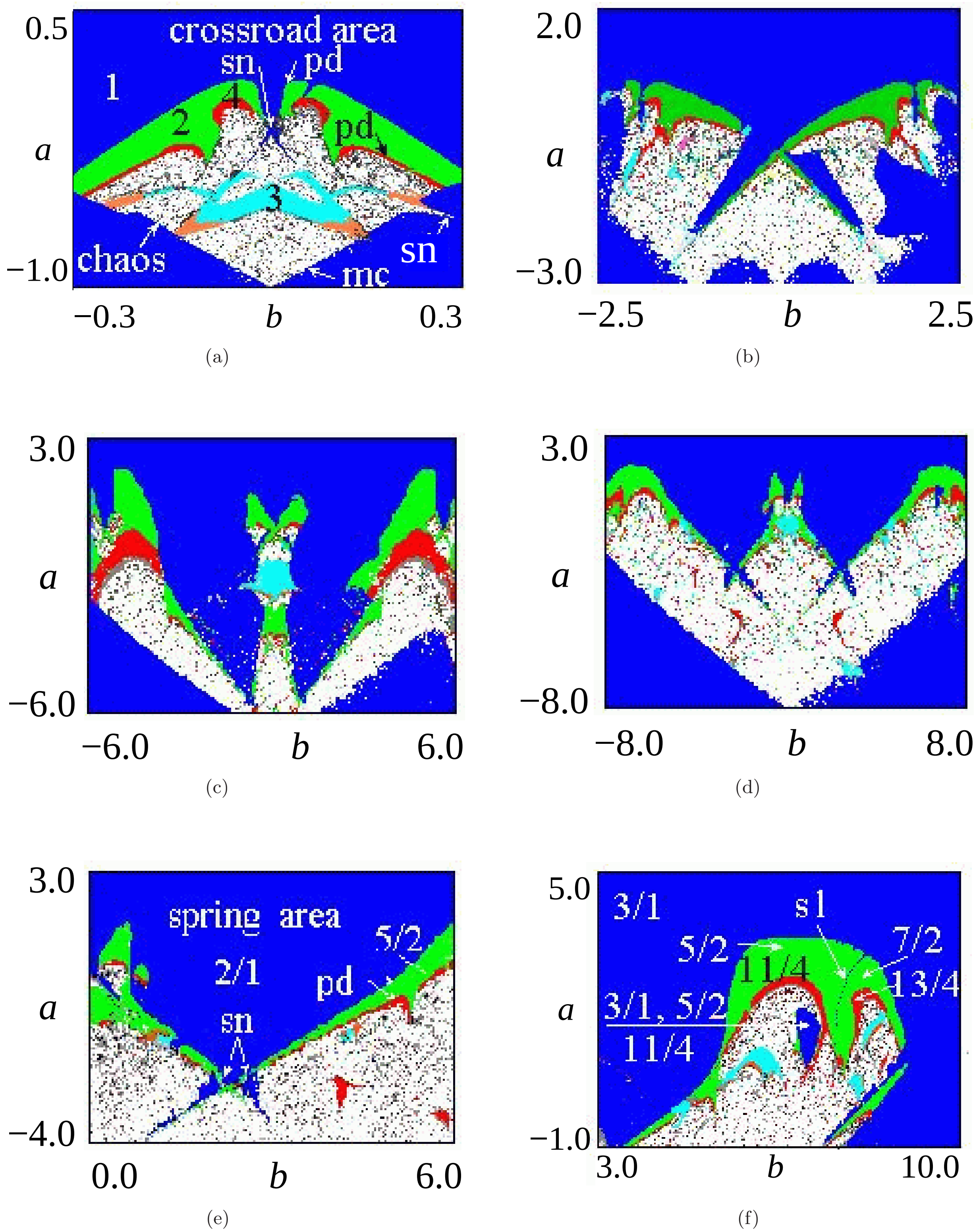

Fig. 12. Development of the dynamical regime topographies for the oscillator (17) on the (b, a)-plane at $k = 0.2$, $\omega = 1.0$ and increasing forcing amplitude B: (a) $B = 0.25$, (b) $B = 3.0$, (c) $B = 6.0$, and (d) $B = 8.0$. (e) Enlarged fragment of Fig. 12(d), (f) enlarged fragment of Fig. 12(d), the broadened inner part of right crossroad area. The "sn" and "pd" abbreviations correspond to the lines of saddle-node bifurcation and to the period-doubling one, the term "mc" to the metastable chaos, and "sl" to the dotted line of the crossroad area separation, respectively. The numbers define the involved subharmonics.

In Fig. 12(a) the topography mapping out the dynamical regimes for Eq. (17) is plotted in the (b, a)-parameter plane. Here the chaotic regions are shown in white, blue regions correspond to period-1 solutions, green color is for period-2 solutions, and other periodic regimes are coded by different colors. We distinguish between three kinds of transitions from the period-1 orbit SO, which corresponds to the oscillations within one of the potential wells only, to a chaotic orbit LO, that covers both wells. (The abbreviations SO and LO were suggested by Szemplinska-Stupnicka [1993] for the small orbit and large orbit, respectively.) The first transition is the period-doubling cascade to chaos at the top of the picture; the second transition proceeds via a saddle-node bifurcation in the middle of the topography; and the last case is the transition through the metastable chaos (where chaotic transients can be observed) in the lower part of Fig. 12(a).

Let us now consider the consequent evolution of the topography in the (b, a)-parameter plane with increasing values of the forcing amplitude B. Starting from the amplitude $B = 0.25$, we can see the crossroad area formed by lines of period-doubling bifurcations and saddle-node bifurcations, located at the top part of Fig. 12(a). The characteristic feature of this structure is the large period-3 window in the lower middle of the figure. Increasing the forcing amplitude B leads to the disappearance of the periodic windows as well as to the expansion of the region of complex dynamics [Fig. 12(b)]. Two spring areas arise along the lines of saddle-node bifurcations and a small crossroad area appears between them [Fig. 12(c)]. Furthermore, the right and left parts of the original configuration are separated by two new crossroad areas, and at $B = 6$, there are already two spring areas in the lower part of Fig. 12(c) and three crossroad areas at the top. The rightmost spring area configuration is formed by lines of period-doubling bifurcations for subharmonics 2/1 and 5/2, shown in detail in Fig. 12(e). With further increase of the amplitude, the left and right crossroad areas are broken into two parts each. The outer parts (nearest to the edge of the picture) are narrow, and the inner parts have become broader [Fig. 12(d)]. The broadened inner part of right crossroad area is shown in detail in Fig. 12(f), where one can see period-doubling bifurcations for the subharmonics 3/1, 5/2 and 11/4 in the left half part, and for the subharmonics 3/1, 7/2 and 13/4 in the right half part. The inner structure of this figure corresponds to the scheme in Fig. 11. The blue dotted line between the left and right halves outlines the direction along which the next separation of the broadened part can occur, leading to the appearance of the next crossroad area. In the left half there is a small spring area formed by bifurcation lines for $3/1, 5/2$ and $11/4$ subharmonics.

Thus, we have described the scenario for the topography evolution with increasing amplitude for the oscillator with cusp catastrophe. It is natural to ask how this scenario will change as the degree of the polynomial potential function increases in Eq. (17). Will these changes have universal character?

Consider the oscillator with a sixth degree polynomial potential function

$$\ddot{x} + k\dot{x} + x^5 + ax + b = B \cos \omega t\,, \tag{18}$$

and the oscillator with eighth degree polynomial potential function

$$\ddot{x} + k\dot{x} + x^7 + ax + b = B \cos \omega t\,. \tag{19}$$

The parameters of Eqs. (18) and (19) were chosen to be the same as for Eq. (17) in order to illustrate the effect dynamics of increasing the order of the polynomial potential function on the system dynamics.

Figures 13(a) and 13(b) for the oscillator (18) reproduce the same dynamics as for the oscillator with cusp catastrophe (17), but for smaller amplitudes. A new feature in the topography evolution arises at $B = 6$ [Fig. 13(c)], when a new spring area appears in the place of the intersection of the saddle-node bifurcations lines of two neighboring spring areas marked in Fig. 13(b). The enlarged right spring area is shown at $B = 8$ in Fig. 13(e). The development of these three spring areas leads to an intersection of their bifurcation lines. Some of the intersections of saddle-node bifurcations lines of these neighboring spring areas are shown in Fig. 13(d). At $B = 8$ the central crossroad area is broken into two crossroad areas, the inner parts of which have broadened while the outer parts have narrowed, as for example above. The same transformations occur for the two crossroad areas in the left and in the right halves of Fig. 13(d). Hence there are four crossroad areas and three spring areas at $B = 8$. Figure 13(f) shows a magnification of part of Fig. 13(d), which illustrates that copies of spring and crossroad areas are found on smaller scales.

Let us now examine the observed scenario for the oscillator (19). The first three figures [see Figs. 14(a)–14(c)] repeat the dynamics of the oscillator (18). In the following we wish to watch the

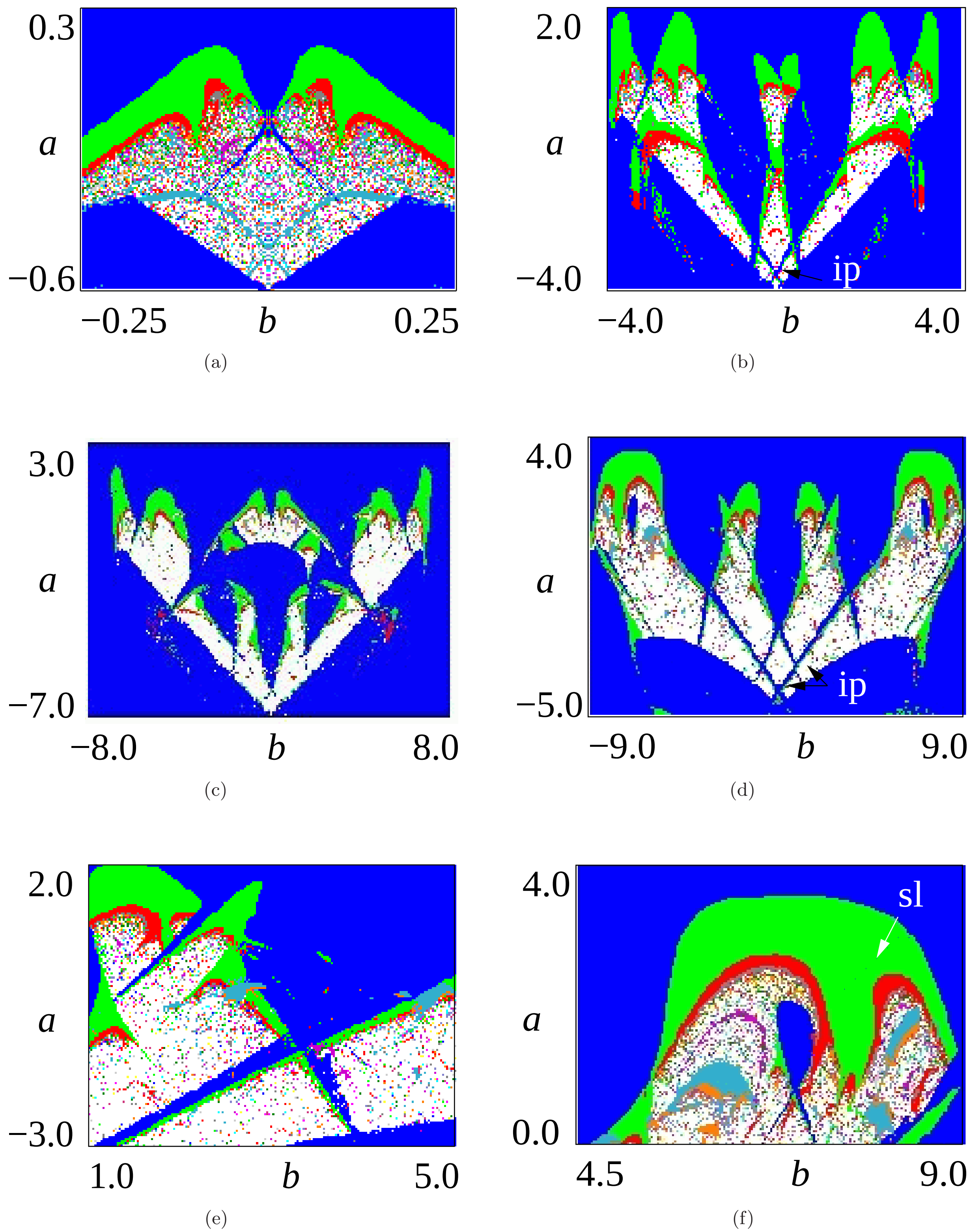

Fig. 13. Development of the dynamical regime topographies for the oscillator (18) on the (b, a)-plane at $k = 0.2$, $\omega = 1.0$ and increasing amplitude B: (a) $B = 0.25$, (b) $B = 3.0$, (c) $B = 6.0$, and (d) $B = 8.0$. (e) Enlarged fragment of Fig. 13(d), (f) enlarged fragment of Fig. 13(d), the broadened inner part of right crossroad area. The "ip" and "sl" abbreviations mark the place of intersection of saddle-node bifurcation lines of neighboring spring areas and the dotted line of the crossroad area separation, respectively.

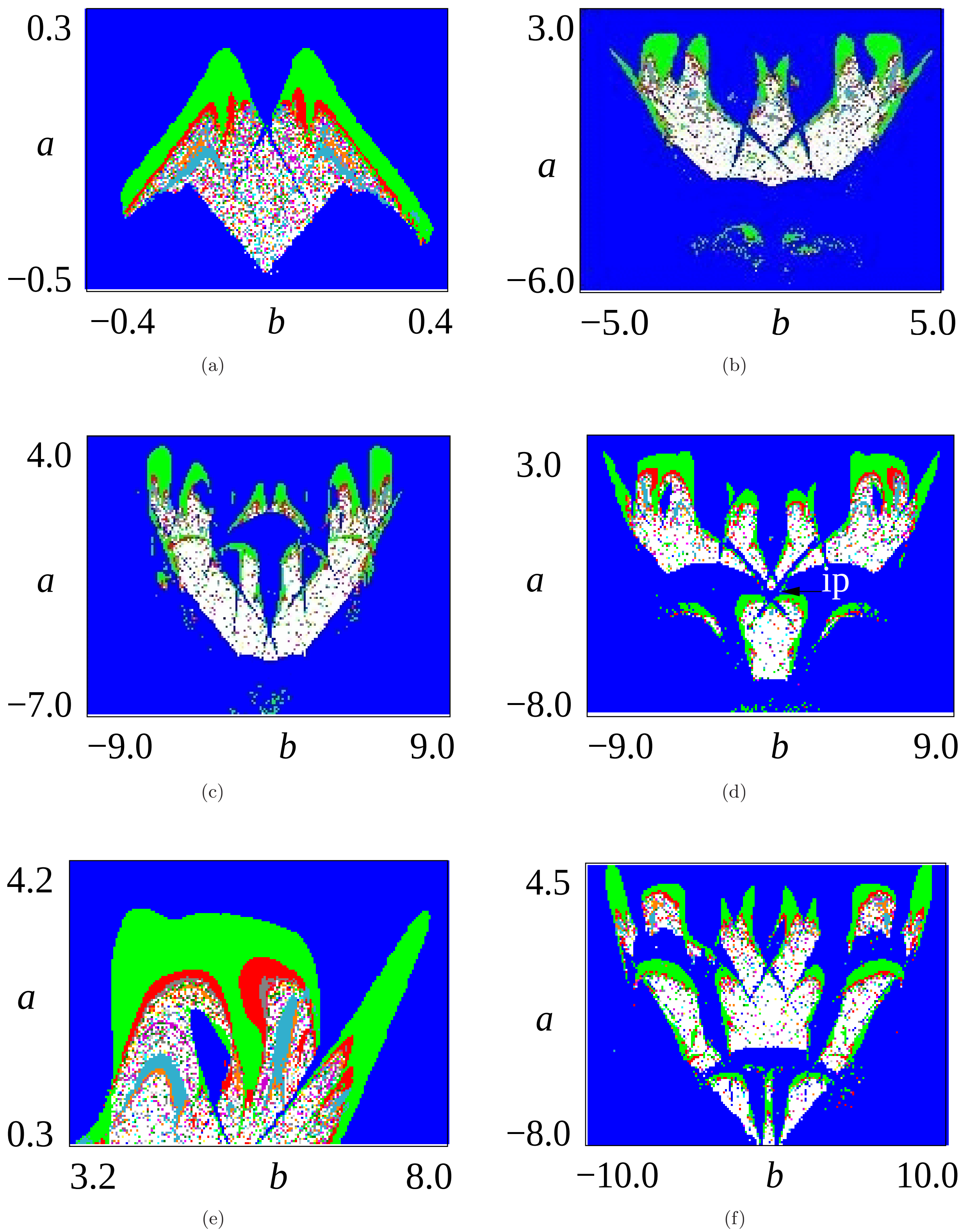

Fig. 14. Development of the dynamical regime charts for the oscillator (19) on the (b, a)-parameters plane at $k = 0.2$, $\omega = 1.0$ and increasing amplitude B: (a) $B = 0.25$, (b) $B = 3.0$, (c) $B = 5.0$, and (d) $B = 6.0$. (e) Enlarged fragment of Fig. 14(d), the broadened inner part of right crossroad area. (f) $B = 7.0$, (g) $B = 8.0$, (h,i) enlarged fragments of Fig. 14(g), (j) enlarged fragment of Fig. 14(g), a new right crossroad area. The "ip" and "sl" abbreviations correspond to the place of intersection of saddle-node bifurcation lines of neighboring spring areas and to the dotted separation line, respectively.

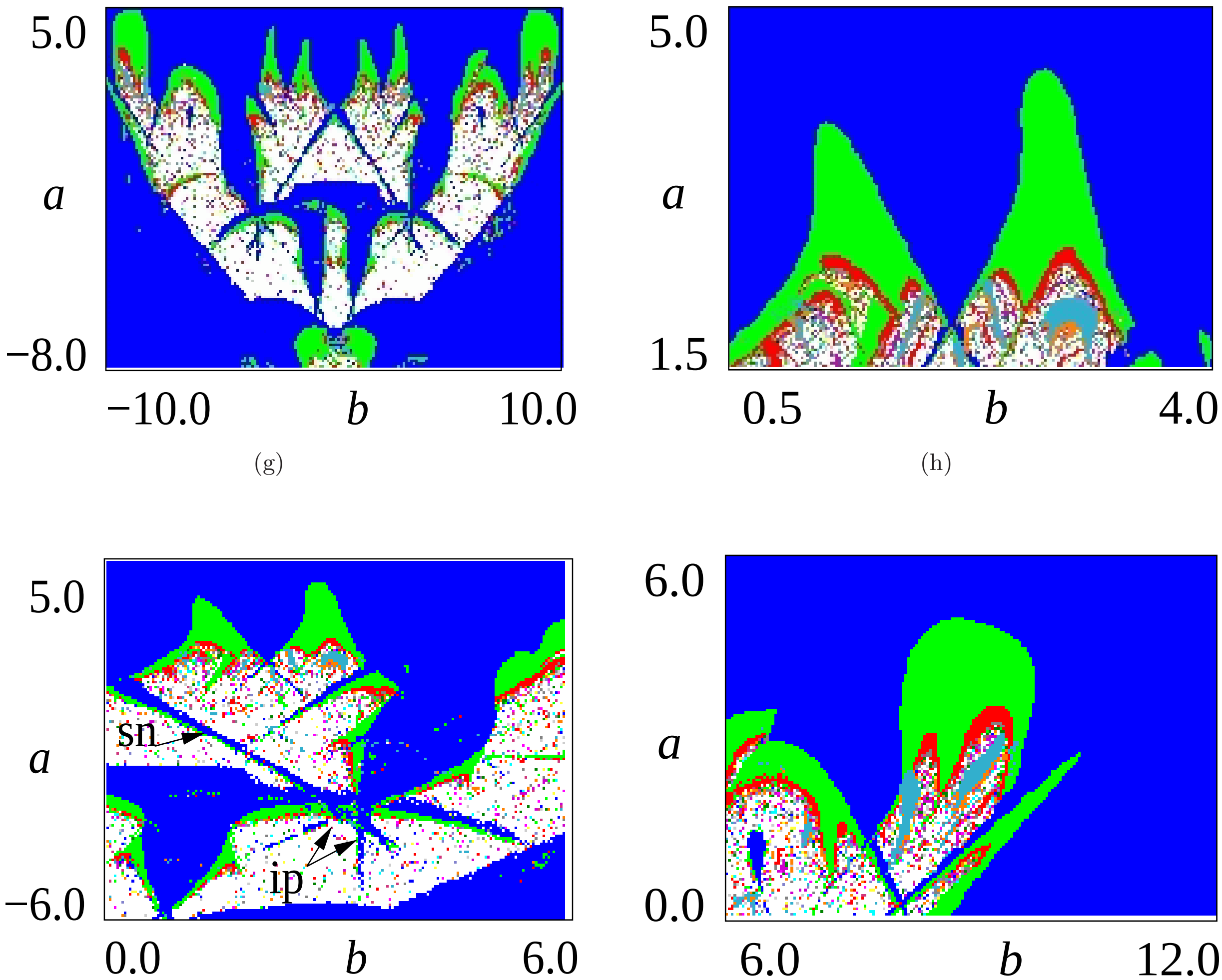

(g) (h) (i) (j)

Fig. 14. (*Continued*)

evolution of the three main characteristic subjects of the chart: the central spring area, the central crossroad area and the right crossroad area. Note that the evolution of the left crossroad area is similar to that observed for the right one.

Further increases of the amplitude makes the central spring area in Fig. 14(c) subject to the following transformations: two new spring areas arise in the place, where its fold lines intersect the fold lines of the neighboring spring areas [see Fig. 14(d); compare with the intersections of fold lines in Fig. 13(d)]. The right spring area is shown in magnification in the lower part of the left half side of Fig. 14(i), where the fold line intersections of the two old spring areas are marked. Moreover, the central crossroad area in Fig. 14(c) is broken down and thus generates two crossroad areas near the top of the center part of Fig. 14(d). Its inner parts are broadened [Fig. 14(f)] and are broken in order to allow a new crossroad area to appear [see Figs. 14(g) and 14(h)]. The same transformations of the right and left crossroad areas are also shown in these figures, where inner parts of the configurations in Fig. 14(d) are broken along the blue dotted line [see Figs. 14(e) and 14(f)] and two crossroad areas are born instead of these parts [see Fig. 14(g)]. The right configuration is shown in Fig. 14(j).

Summarizing the above mentioned results, we have studied the evolution of the topography of dynamical regimes for the oscillators with polynomial potential function of fourth, sixth and eighth degrees (17)–(19). Some conclusions may be drawn about the general features of the evolution of the topography for the oscillators with the polynomial potential function of pth degree, where p is an even number $p > 2$. The described universal scenario of the topography evolution consists in the following. The crossroad areas expand significantly when increasing the forcing amplitude, its right and left parts become separated and generate two new crossroad areas. Two spring areas arise along the lines of saddle-node bifurcations, and one crossroad area arises between them. The new area configurations then appear in the places, where the fold lines of the spring area intersect fold lines of the neighboring configurations. The inner parts of right and left crossroad areas are broadened and broken in order for new crossroad areas to appear instead of the old parts. The higher the degree of the polynomial potential function, the smaller the values of the forcing amplitude are for which the above scenario takes place. Hence, the scenario repeats itself several times (cascade-like) over the considered range of the forcing amplitude, leading to a significant complication of the topography.

The described topographies of the dynamical regimes do not change significantly at other values of the forcing frequency, thus, the scenario of the topography evolution has a universal character for the considered nonlinear oscillators. The approach of the catastrophe theory helps us to understand a intuitive reason for this universality of the oscillator dynamics. The parametrization of Eq. (18) corresponds to one of the sections of the butterfly catastrophe parameter space [Bröcker & Lander, 1975]. Woodcock and Poston showed that this section is typical to the cusp catastrophe: there are fold lines emanating from cusp point on the (a, b)-plane [Woodcock & Poston, 1974]. The parametrization of the next considered Eq. (19) corresponds to the section of the star catastrophe parameter space, where all parameters of the potential at coordinate in higher than second degree equal to zero [Woodcock & Poston, 1974]. In this case the section is typical to a butterfly catastrophe with fold lines, emanating from a cusp point on the (a, b)-plane. Woodcock and Poston remarked that each higher order catastrophe, when plotted on the appropriate plane, generate the relevant lower order catastrophes. Thus, it seems that in our study one picture of the topography evolution is observed in different cases of the projections of the higher order catastrophes on the relevant plane. The speed of the scenario depends on order of the catastrophe. For the oscillators with cusp catastrophe and butterfly catastrophe the speed is smaller than for one with star catastrophe, because the angle between fold lines on the (a, b)-plane for oscillators (17)–(19) gradually decreases. Thus, if there is a particular type of the low order catastrophe in the sections of different higher order catastrophes, then we can expect one scenario of the topography evolution for the corresponding oscillators.

3.2. *Dynamics of nonlinear oscillator with butterfly catastrophe*

In the above discussion we have considered the dynamics of the oscillator with butterfly catastrophe with zero parameters at the coordinates in higher than first degree. We now turn to the consideration of the full parameter space for the nonlinear oscillator with butterfly catastrophe

$$\ddot{x} + k\dot{x} + x^5 + ax^3 + bx^2 + cx + d = B \cos \omega t\,. \tag{20}$$

The corresponding potential function (13) as shown in Table 2 depends on the four controlling parameters a, b, c, and d. Variation of these parameters leads to potential function transformations as shown in Fig. 15. For the correspondence between the forms of the potential (13) and the regions of the sections of the butterfly set see the book by Saunders [1980].

Let us consider the physical example of a magneto-elastic beam inclined in a field from three magnets, described by Eq. (7) in Table 1 with a sixth-order polynomial function. This potential function has three potential wells [Li & Moon, 1990]. Equation (7) is a Duffing type equation with nonlinearity up to fifth order in x, here x_0 is a dimensionless quantity that represents the ratio of the unstable and stable equilibrium positions of the beam. Introducing the parameter $a = x_0^2$, we obtain the example of the oscillator with the butterfly catastrophe.

In Fig. 16(a) the topography of the dynamical regimes for this system is presented in the plane of the forcing amplitude and the parameter a. One can observe curves of period-doubling bifurcations, and the period-doubling cascade to chaos. We now rewrite Eq. (7) in the form

$$\ddot{x} + k\dot{x} + x^5 - (a+1)x^3 + ax + b = B \cos \omega t\,, \tag{21}$$

which corresponds to the addition of an external homogeneous field, with a "tension" b. The potential

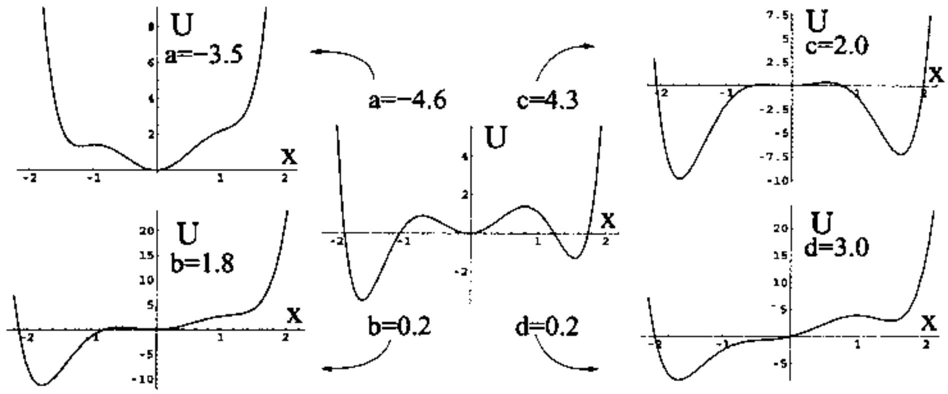

Fig. 15. Transformations of the potential function (13) under variation of the parameters a, b, c, and d.

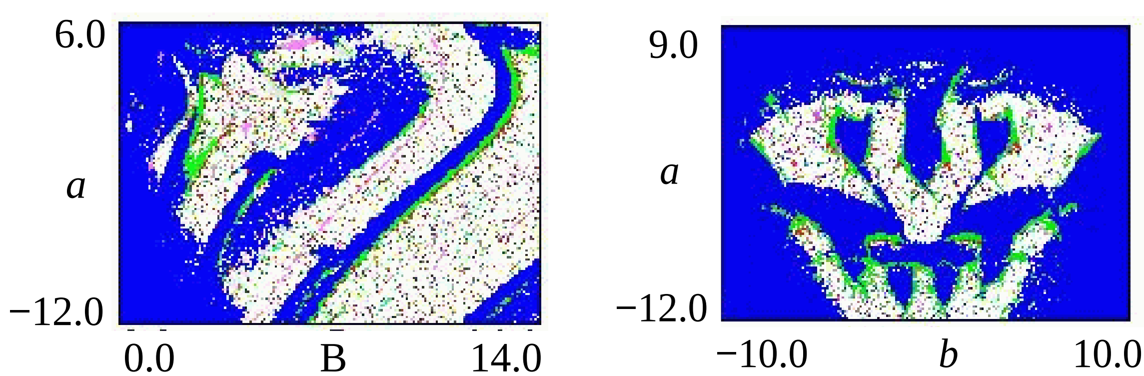

(a) (b)

Fig. 16. The dynamical regimes topography for the oscillator with butterfly catastrophe at $k = 0.2$ and $\omega = 1.0$ in cases for (a) Eq. (7), (b) Eq. (21) at $B = 8.0$.

function for Eq. (21) is given by

$$U(x) = \frac{x^6}{6} - (a+1)\,\frac{x^4}{4} + a\,\frac{x^2}{2} + bx\,, \qquad (22)$$

which has three potential wells and corresponds to the two-parameter section of the butterfly catastrophe parameter space. The topography of the dynamical regimes on the (b, a)-parameter plane for this equation is shown in Fig. 16(b). At $B = 8$ there are four spring areas in the bottom part of the figure and three spring areas in the top one.

Now return to the equation of the oscillator with butterfly catastrophe (20). The two-well potential system possesses homoclinic orbits. A distinct feature of the three-well potential system is that besides homoclinic orbits, it also possesses heteroclinic orbits [Li & Moon, 1990]. Bifurcations involving the homoclinic and heteroclinic orbits lead to complicated intersections of the stable and unstable manifolds. Therefore the basin boundaries will become extremely complicated, in particular, they will become fractal. Let us fix parameters a, b, c, d and consider the basin transformations for different values of the forcing amplitude. Increasing of forcing amplitude from $B = 0.3$ to $B = 1.4$ results in the merger of the four basins into two basins (Fig. 17). If the value of the controlling parameter is smaller than the critical value for the homoclinic bifurcation [Li & Moon, 1990], then the boundaries are clearly smooth, as shown in Fig. 17(a). Else segments of the basin boundaries become nonsmooth or fractal [see Fig. 17(b)]. If initial conditions are chosen near the fractal basin boundaries with a small uncertainty in this case, then the final state to which the motion is attracted is not predictable. With a further increase in parameter

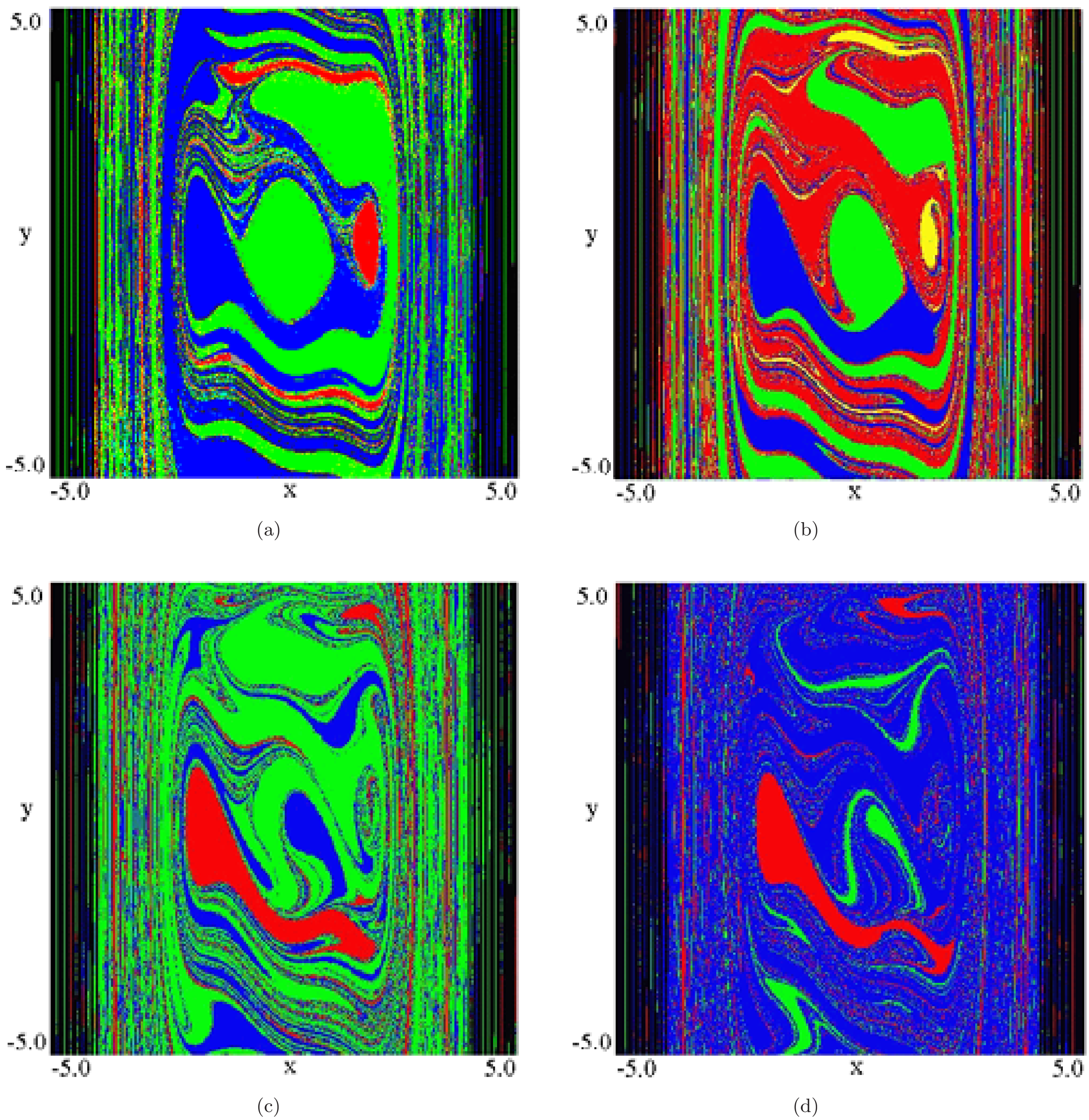

Fig. 17. The basin transformation for the oscillator with butterfly catastrophe (20) at $a = -4.6$, $b = 0.2$, $c = 4.3$, $d = 0.2$, $k = 0.2$, $\omega = 1.0$ and increasing amplitude B: (a–c) $B = 0.3$, $B = 0.6$, $B = 1.0$ — four attractors, and (d) $B = 1.2$ three only.

B, the fractal basin boundaries spread out and become more complex, as shown in Fig. 17(c). This fractalization leads to the incursion of the fragments of others basins and to the merger of some neighboring basins [see Fig. 17(d)]. At $B = 1.4$ the system has only two attractors rather than the previous four. Hence a transition from the oscillations within one of the wells of the three-well potential to oscillations which spread out over all three wells takes place.

Consider the variation of parameters a, b, c, and d corresponding to the potential function (13) transformations presented in Fig. 15. Increasing the value of the parameter a, say, from $a = -5.0$ to $a = -4.2$

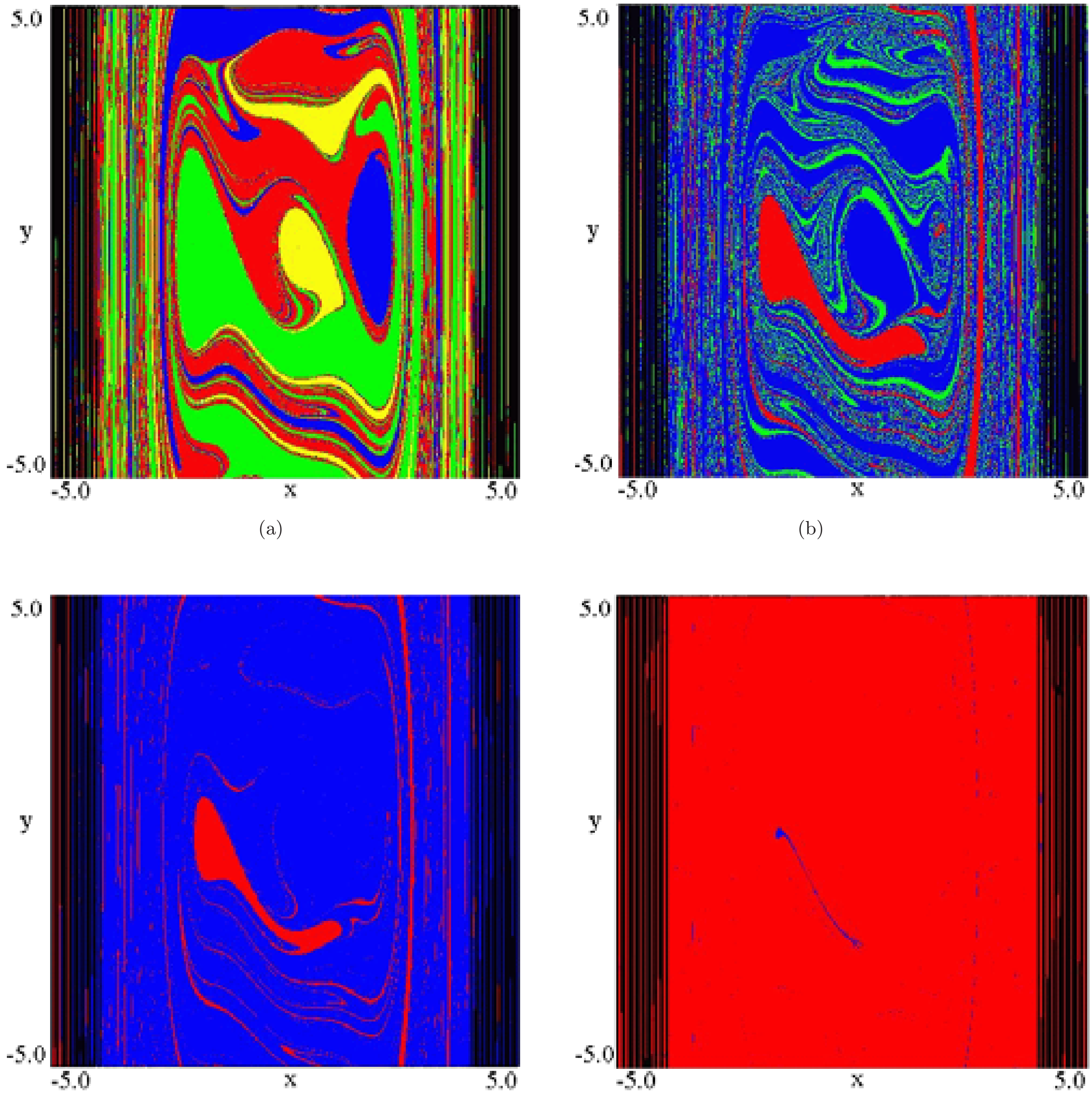

Fig. 18. The basin transformation for the oscillator with butterfly catastrophe (20) at $b = 0.2$, $c = 4.3$, $d = 0.2$, $k = 0.2$, $\omega = 1.0$, $B = 0.8$ and increasing parameter a: (a) $a = -5.0$ four attractors, (b) $a = -4.5$ three attractors, (c) $a = -4.4$, (d) $a = -4.2$ two attractors.

(while the remaining parameters are fixed) leads to the merger of the four basins of different attractors into two basins [see Figs. 18(a)–18(d)]. The same basin transformation occurs when increasing the parameters b and d from 0.2 (four attractors) to 0.25 (three attractors), and to 0.3 (two attractors), or decreasing the parameter c from 3.5 (four attractors) to 3.2 (three attractors), and to 1.0 (two attractors). The basins of attraction for increasing b are similar to the basins for increasing d. There is one

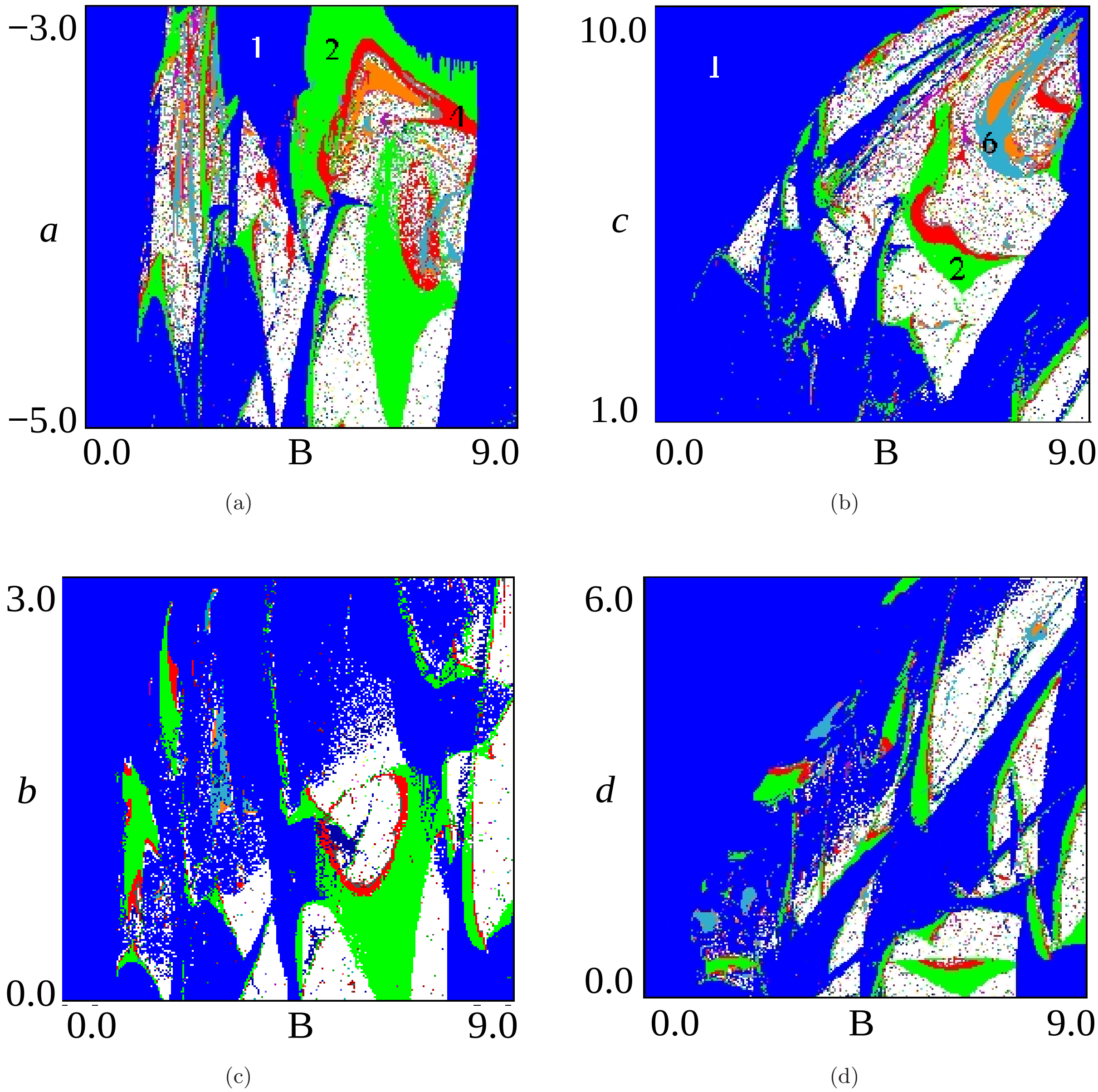

Fig. 19. Charts of the dynamical regimes for the oscillator with butterfly catastrophe (20) on the plane of forcing amplitude B and potential function parameters at $k = 0.2$, $\omega = 1.0$, (a) $b = 0.2$, $c = 4.3$, $d = 0.2$, (b) $a = -4.6$, $b = 0.2$, $d = 0.2$, (c) $a = -4.6$, $c = 4.3$, $d = 0.2$, (d) $a = -4.6$, $b = 0.2$, $c = 4.3$.

attractor only in the cases of $a > -4.1$, or $b > 3.0$, or $d > 0.9$. Thus, a transition from oscillations in the three-well potential to oscillations in a one-well potential takes place.

Figures 17 and 18 were obtained for the forcing amplitude parameter value $B = 0.8$. All attractors, the basins of which were presented in these figures, are period-1 cycles. The evolution of these regimes with increasing forcing amplitude is illustrated in Fig. 19. The dynamical regime charts are presented for the oscillator with butterfly catastrophe (20) in the (B, a)-, (B, c)-, (B, b)- and (B, d)-parameter planes. One can see the period-doubling cascade to chaos on these topographies [Figs. 19(a)–19(d)]. In Fig. 20 the dynamical regimes topographies on the potential function parameter plane can be seen. The topography on the plane of the (d, a) parameters exhibits at least one crossroad area, based on the subharmonic solution 6/3, and spring areas based on the subharmonics 6/3 and 2/1 [see Figs. 20(c) and 20(d)]. The topography of the plane of (d, c) parameters has a crossroad area, based on the sub-

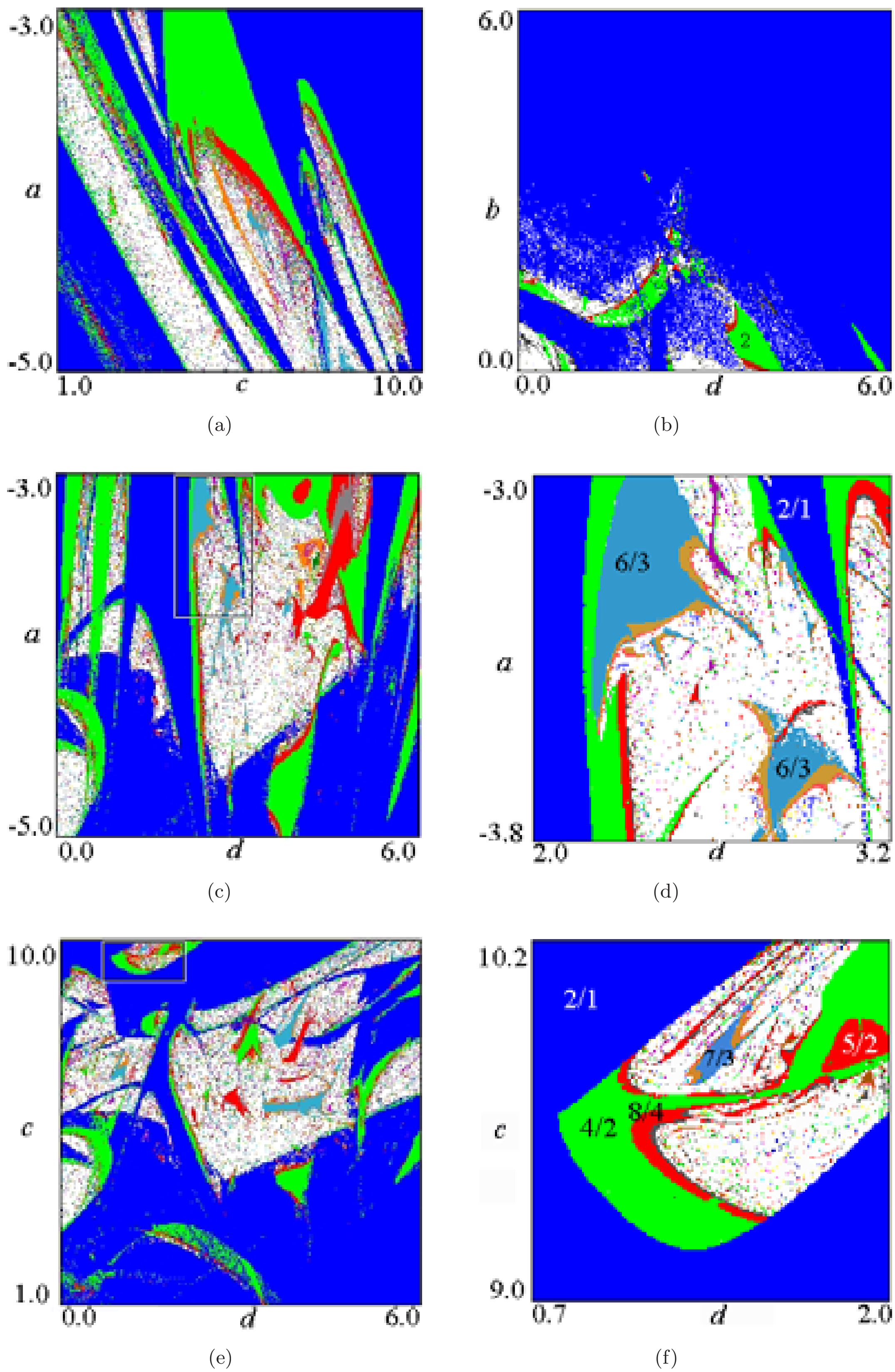

Fig. 20. Charts of the dynamical regimes for the oscillator with butterfly catastrophe (20) on the plane of potential function parameters at $k = 0.2$, $\omega = 1.0$, $B = 5.0$, (a) $b = 0.2$, $d = 0.2$, (b) $a = -4.6$, $c = 4.3$, (c) $b = 0.2$, $c = 4.3$. (d) Enlarged fragment of Fig. 20(c). (e) $a = -4.6$, $b = 0.2$. (f) Enlarged fragment of Fig. 20(e). The numbers define the involved subharmonics.

harmonic 4/2, and a spring area of the subharmonic 7/3 [see Figs. 20(e) and 20(f)].

Thus, the oscillator with butterfly catastrophe demonstrates the dependence of the dynamics on potential function parameters. The basins merge at the variation of these parameters, and there are the crossroad area and spring area configurations on the plane of these parameters.

4. Conclusions

In the present work the behavior of nonlinear oscillators was considered. A new classification of oscillators was developed based on the scheme of Thom's catastrophe theory. This allowed us to describe the oscillators in Table 1, which differ from each other in the order of the potential functions and in the possibility of escape, by using only one equation. All previous examples are particular cases of this oscillator equation with some elementary catastrophe taken at different fixed values of the controlling parameters. We studied the behavior of this more general model equation in the full parameter space. At the end result, we have discovered the universal properties of the dynamics of systems with Thom's catastrophe unfoldings in the context of forced oscillators.

First, an investigation of the systems which possess escaping solutions was carried out. For the oscillators with fold, dual cusp and swallowtail catastrophes the dependence of the dynamics on the parameters of the potential function was described. Variation of the potential function parameters leads to the basin erosion. The escape region and the region of stable solutions were estimated on the charts of the dynamical regimes in the space of the control parameters. The dependence of the location of the fractal escape boundary on the variation of the parameters of the potential function was illustrated.

Second, for the oscillators with nonescaping solutions the evolution of the dynamical regime topographies under the increase of the forcing amplitude was considered. We compared the evolution of the topographies for oscillators with the polynomial potential function of fourth, sixth and eighth degrees, corresponding to the cusp, butterfly and star catastrophes. It seems that the crossroad area and spring area configurations arise at smaller amplitudes in case of higher degree of the polynomial potential function. We found one universal scenario of the developing of these configurations in the plan of the potential function parameters with increase of the forcing amplitude. For every considered oscillator the initial crossroad areas expand and become separated leading to the generation of two new crossroad areas on the right and on the left of the chart. Moreover, along the lines of saddle-node bifurcations of the initial crossroad area two spring areas arise, and the new area configurations then appear in the places, where the fold lines of the neighboring spring areas intersect themselves. The inner parts of the right and left crossroad areas are broadened and broken in order for new crossroad areas to appear instead of the old parts. This universal scenario repeats itself several times on the regarded range of the forcing amplitude leading to the complication of the topographies. The higher the degree of the potential function, the higher the speed of the repetition of this scenario. The scenario was described for the oscillators with some higher order catastrophes, which have cusp catastrophe in one particular section. We suppose that consideration of other sections may be of the same interest. For the oscillators with the higher order catastrophes which have another lower order catastrophe in the sections also, some universal features of the topography evolution can observed.

We have shown for the oscillator with butterfly catastrophe, as the example of the higher order catastrophe, that the basin transformations take place for the variation of the potential function parameters as well for the increasing of the forcing amplitude. The topographies of the dynamical regimes on the plane of the potential function parameters demonstrate also the crossroad area and spring area configurations.

Acknowledgments

This work is supported, in part, by RFBR, grant 00-02-17509 and by RFBR, grant 01-02-06390. A. Kuznetsova acknowledges support from Danish Graduate School in Nonlinear Science to visit The Technical University of Denmark, where a part of this work has been done. A. Kuznetsov and A. Kuzentsova acknowledge support via the Research and Educational Center of Nonlinear Dynamics and Biophysics of Saratov State University from CRDF, award No REC–006. A. Kuznetsova appreciates the useful discussions with I. Sataev, and gratefully acknowledges discussion with U. Parlitz during the seminar in Max Planck Institute for the Physics of Complex Systems in Dresden. For useful comments, advice and information relating to the present study A. Kuznetsova thanks N. Kopell and J. Guckenheimer.

References

Arnold, V. I., Afrajmovich, V. S., Il'yashenko, Yu. S. & Shilnikov, L. P. [1999] *Bifurcation Theory and Catastrophe Theory* (Springer-Verlag, NY).

Bröcker, Th. & Lander, L. [1975] *Differentiable Germs and Catastrophes* (Cambridge University Press, Cambridge).

Carcasses, J. P. & Mira, C. [1991] "Crossroad area — spring area transition (I) parameter plane representation," *Int. J. Bifurcation and Chaos* **1**, 183–196.

Duffing, G. [1918] *Erzwungene Schwingungen bei veranderlicher Eigenfrequenz und ihre technische Bedeutun* (Vieweg, Braunschweig).

English, V. & Lauterborn, W. [1991] "Regular window structure of a double-well Duffing oscillator," *Phys. Rev.* **A44**, 916–924.

Flytzanis, Chr. & Tang, C. L. [1980] "Light-induced critical behavior in the four-wave interaction in nonlinear systems," *Phys. Rev. Lett.* **45**, p. 441.

Gallas, J. A. C. & Catarina, S. [1993] "Structure of the parameter space of Henon map," *Phys. Rev. Lett.* **70**, 2714–2717.

Goldstone, J. A. & Garmire, E. [1984] "Intrinsic optical bistability in nonlinear media," *Phys. Rev. Lett.* **53**, 910–913.

Goryachenko, V. D. [1995] *Elementy Teorii Kolebaniy* (*Elements of the Oscillation Theory*) (Krasnoyarskiy University Press, Kpasnoyarsk), (in Russian).

Guckenheimer, J. & Holmes, P. [1983] *Nonlinear Oscillations, Dynamical Systems and Bifurcations of Vector Fields* (Springer-Verlag, NY).

Hayashi, C. [1964] *Nonlinear Oscillations in Physical Systems* (McGraw-Hill, NY).

Hayashi, C. & Ueda, Y. [1973] "Behavior of solutions for certain types of nonlinear differential equations of the second order," *Proc. Fifth Int. Conf. Nonlinear Oscillations*, 1973, Poznan, Vol. 14, pp. 341–351.

Huberman, B. A. & Crutchfield, J. P. [1979] "Chaotic states of anharmonic systems in periodic fields," *Phys. Rev. Lett.* **43**, 1743–1747.

Huberman, B. A., Crutchfield, G. P. & Packard, N. H. [1980] "Noise phenomena in Josephson junctions," *Appl. Phys. Lett.* **37**, 750–752.

Kao, Y. H., Huang, J. C. & Gou, Y. S. [1988] "Routes to chaos in the Duffing oscillator with a single potential well," *Phys. Lett.* **A131**, 91–97.

Klinker, T., Meyer-Ilse, W. & Lauterborn, W. [1984] "Period doubling and chaotic behavior in a driven Toda oscillator," *Phys. Lett.* **A101**, 371–375.

Kloster, N. & Knudsen, C. [1995] "Bifurcations near 1:2 subharmonic resonance in a structural dynamics model," *Chaos Solit. Fract.* **5**, 50–66.

Komuro, M., Tokunaga, R., Matsumoto, T., Chua, L. & Hotta, A. [1991] "Global bifurcation analysis of the double scroll circuit," *Int. J. Bifurcation and Chaos* **1**, 139–182.

Kuznetsov, A. P. & Potapova, A. Yu. [2000] "Features of the complex dynamics of the nonlinear oscillators with Thom catastrophes," *Izvestiya Vyzov. Appl. Nonlin. Dyn.* **8**, 94–120, (in Russian).

Li, G. X. & Moon, F. C. [1990] "Criteria for chaos of a three-well potential oscillator with homoclinic and heteroclinic orbits," *J. Sound Vibr.* **136**, 17–34.

Lu, Y.-C. [1976] *Singularity Theory and an Introduction to Catastrophe Theory* (Springer-Verlag, NY).

MacDonald, A. H. & Plischke, M. [1983] "Study of the driven damped pendulum: Application to Josephson junctions and charge-density-wave systems," *Phys. Rev.* **B27**, 201–211.

Mackey, R. S. & Tresser, C. [1987] "Some flesh on the skeleton: The bifurcation structure of bimodal maps," *Physica* **D27**, 412–422.

Marzec, C. J. & Spiegel, E. A. [1980] "Ordinary differential equations with strange attractors," *J. Appl. Math.* **38**, 403–421.

Mira, C. & Carcasses, J. [1991] "On the crossroad area — saddle area and spring area transition," *Int. J. Bifurcation and Chaos* **1**, p. 643.

Mitra, S. & Sinha, D. U. [1981] "Catastrophe theory in some aspects of earth sciences," in *Catastrophe Theory and Applications*, ed. Sinha, D. U. (John Wiley, NY).

Moon, W. & Holmes, P. J. [1979] "A magnetoelastic strange attractor," *J. Sound Vibr.* **65**, 285–296.

Mosekilde, E. [1996] *Topics in Nonlinear Dynamic* (World Scientific, Singapore).

Neimark, Yu. I. & Landa, P. S. [1987] *Stohasticheskije i Haoticheskije Kolebaniya* (*Stochastic and Chaotic Oscillations*) (Nauka, Moscow), (in Russian).

Parlitz, U. [1991] "Common dynamical features of periodically driven strictly dissipative oscillators," *Int. J. Bifurcation and Chaos* **3**, 703–715.

Petersson, J. [1990] "Chaos new structural phase transition," *Z. Naturforschung* **A45**, 958–964.

Poston, T. & Stewart, I. [1978] *Catastrophe Theory and its Applications* (Pitman, London).

Saunders, P. T. [1980] *An Introduction to Catastrophe Theory* (Cambridge University Press, NY).

Scheffczyk, C., Parlitz, U., Kurz, T., Knop, W. & Lauterborn, W. [1991] "Comparison of bifurcation structures of driven dissipative nonlinear oscillators," *Phys. Rev.* **A43**, 6495–6502.

Soliman, M. S. & Thompson, J. M. T. [1991] "Transient and steady state analysis of capsize phenomena," *Appl. Ocean Res.* **13**, 82–92.

Soliman, M. S. [1994] "Predicting regimes of indeterminate jumps to resonance by assessing fractal boundaries in control space," *Int. J. Bifurcation and Chaos* **4**, 1645–1653.

Swift, J. W. & Wiesenfeld, K. [1984] "Suppression of period doubling in symmetric systems," *Phys. Rev. Lett.* **52**, 705–708.

Szemplinska-Stupnicka, W. [1993] "Steady states in the twin potential oscillator: Computer simulations and approximate analytical studies," *Chaos* **3**, 375–385.

Thompson, J. M. & Stewart, H. B. [1986] *Nonlinear Dynamics and Chaos* (Wiley, NY).

Thompson, J. M. T., Bishop, S. R. & Leung, L. M. [1987] "Fractal basins and chaotic bifurcations prior to escape from the potential well," *Phys. Lett.* **A121**, 116–120.

Thompson, J. M. T. [1995] "Chaos and fractal basin boundaries in engineering," in *The Nature of Chaos*, ed. Mallin, T. (Clarendon Press, Oxford).

Ueda, Y. [1991] "Survey of regular and chaotic phenomena in the forced Duffing oscillator," *Chaos Solit. Fract.* **1**, 199–231.

Ueda, Y. [1992] "Strange attractors and the origin of chaos," *Nonlin. Sci. Today* **2**, 1–16.

Woodcock, A. E. R. & Poston, T. [1974] *A Geometrical Study of the Elementary Catastrophes*, Lecture Notes in Mathematics, Vol. 373 (Springer-Verlag, Berlin).

Woodcock, A. & Davis, M. [1991] *Catastrophe Theory* (Penguin Books, London).